PEG-COATED Fe_3O_4 FOR Li-ION BATTERY ANODES: EFFECTS OF CRYSTALLITE SIZE AND SURFACE CHEMISTRY

A Thesis
Presented to
The Academic Faculty

By

Krysten Minnici

In Partial Fulfillment
Of the Requirements for the Degree
Masters of Science in Chemical & Biomolecular Engineering

Georgia Institute of Technology

May 2017

PEG-COATED Fe_3O_4 FOR Li-ION BATTERY ANODES: EFFECTS OF CRYSTALLITE SIZE AND SURFACE CHEMISTRY

Approved by:

Dr. Elsa Reichmanis, Advisor
School of Chemical & Biomolecular Engineering
Georgia Institute of Technology

Dr. Thomas Fuller
School of Chemical & Biomolecular Engineering
Georgia Institute of Technology

Dr. Carson Meredith
School of Chemical & Biomolecular Engineering
Georgia Institute of Technology

Date approved: May 2017

ACKNOWLEDGEMENTS

I would first like to thank my advisor, Dr. Elsa Reichmanis, for her continued guidance and support. I would also like to thank my Thesis Committee: Dr. Thomas Fuller and Dr. Carson Meredith. The Reichmanis group has also been essential to the completion of this thesis, particularly, Yo Han Kwon for his expertise in lithium-ion batteries and patience when teaching me important electrochemical techniques used throughout this work. Additionally, I would like to thank Bailey Risteen, Mike McBride and Brian Khau, other group members, for help with revising this work and discussing various results. I would also like to extend my appreciation to the Fuller lab for use of their facilities to fabricate coin cells and conduct impedance testing. Last, but certainly not least, I would like to thank my family, especially my parents, for their endless support and encouragement.

TABLE OF CONTENTS

Page

LIST OF TABLES

Page

LIST OF FIGURES

Page

LIST OF SYMBOLS AND ABBREVIATIONS

C	carbon
DEC	diethylene carbonate
DLS	Dynamic light scattering
EC	ethylene carbonate
EDS	energy dispersive x-ray spectroscopy
EIS	Electrical impedance spectroscopy
Fe_3O_4	iron oxide, magnetite
FE-SEM	field-emission scanning electron microscopy
FTIR	Fourier transform infrared
g	gram(s)
Hz	Hertz
KBr	Potassium bromide
kDa	kiloDalton
$LiPF_6$	Lithium hexafluorophosphate
mAh g^{-1}	milliampere hour per gram
MHz	megaHertz
min	minute(s)
mL	milliliter(s)
NH_4OH	ammonium hydroxide
NMP	N-methyl-2-pyrrolidone
PEG	polyethylene glycol

PEG-Fe_3O_4	Fe_3O_4 particles coated with polyethylene glycol
PPBT	poly[3-potassium-4-butanoate] thiophene]
PVDF	poly(vinylidene difluoride)
rpm	revolutions per minute
s	second(s)
TEM	Transmission electron microscopy
TGA	Thermogravimetric Analysis
W	watt(s)
w/v	weight/volume percent
XPS	X-ray spectroscopy
XRD	X-ray powder diffraction

SUMMARY

Battery electrodes are complex mesoscale systems comprised of an active material, conductive agent, current collector, and polymeric binder[1]. Previous work focused on enhancing electron and ion transport in high capacity anode systems by introducing poly[3-(potassium-4-butanoate) thiophene] (PPBT) as a binder component and a polyethylene glycol (PEG) surface coating on magnetite (Fe_3O_4) nanoparticles[2]. The PPBT/PEG system will be utilized in this work, which takes a closer look at the active material, Fe_3O_4, and examines the effects of surface chemistry and crystallite size (10 nm vs. 20 nm) on battery performance.

Variations in surface chemistry are due to the synthesis methods used for Fe_3O_4, which use ammonium hydroxide or triethylamine as a base. XRD and TEM initially characterized the active materials to confirm the magnetite phase and crystallite size. DLS and zeta potential measurements demonstrated aggregate size and colloidal stability. SEM images of the electrodes, which are composed of Fe_3O_4 particles, carbon additives, and the PPBT binder, indicate that the bases produce different morphologies. The Fe_3O_4 particles synthesized with ammonium hydroxide appear more dispersed relative to those made with triethylamine, which could have a significant impact on the battery performance. Furthermore, XPS and FTIR data indicate that these bases produce difference chemical interactions within the electrode.

Electrochemical testing demonstrates that the triethylamine-based electrode has a higher capacity and better capacity retention over 100 cycles at 0.3C as compared to the ammonium hydroxide-based electrode. With regards to differences in active material size, the electrodes with 20 nm crystallite size Fe_3O_4 initially have a higher capacity, but the electrodes with 10 nm crystallite size Fe_3O_4 have better capacity retention over 100 cycles at 0.3C. Rate capability

testing and electrical impedance confirm the superior performance of triethylamine derived electrodes and the 10 nm crystallite size.

CHAPTER 1 : INTRODUCTION

1.1 Overview

Lithium-ion batteries are one of the most important energy storage devices used for various applications, but challenges exist to meet demands for high density energy storage[3,4]. The underlying science behind battery technology is often criticized for its slow advancement[5]. New battery technologies are rare and as such, the energy density of lithium-ion batteries has increased only 8-9% per year since the 1990s[6]. However, lithium ion batteries have replaced other energy storage device chemistries, especially in the mobile electronics market[7]. Much research is focused on improving both energy and power density and moving towards the top right corner of the Ragone plot (Figure 1-1). Clearly, lithium ion batteries have the highest combined energy density and power density available from existing rechargeable battery technologies, but are still behind the demands of the consumer[8].

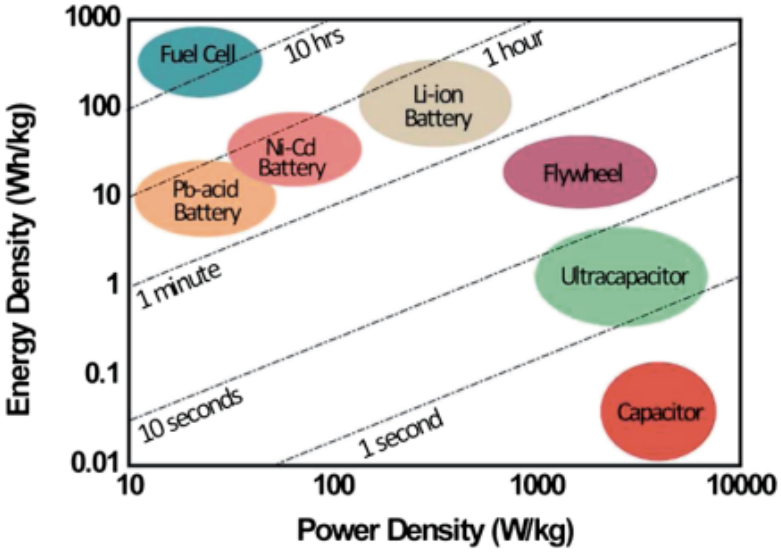

Figure 1-1: Ragone plot for different energy storage technologies. [Reproduced with the permission of the author[9].]

The working principle of a lithium-ion battery is based on reversible intercalation and de-intercalation of the lithium ions, Li^+, into electrodes[7], which is illustrated in Figure 1-2. The cell is composed of positively and negatively charged electrodes, separated by an electrolyte, which enables ion transfer between the electrodes[5]. The electrodes (Figure 1-3) are complex mesoscale systems comprised of an active material, conductive agent, current collector, and polymeric binder[1]. The polymeric binder serves to improve adhesion, mechanical strength and ease of processing[7]. The electrodes are divided by a microporous separator film, which is infused with the electrolyte. During the first cycle, the organic electrolyte decomposes to form a solid electrolyte interface (SEI) layer on the surface of the electrodes[7]. The electrode materials are crucial to determine the capacity and power density of the lithium-ion battery, whereas the capacity retention is governed by the quality and stability of the interfaces within the electrode system.

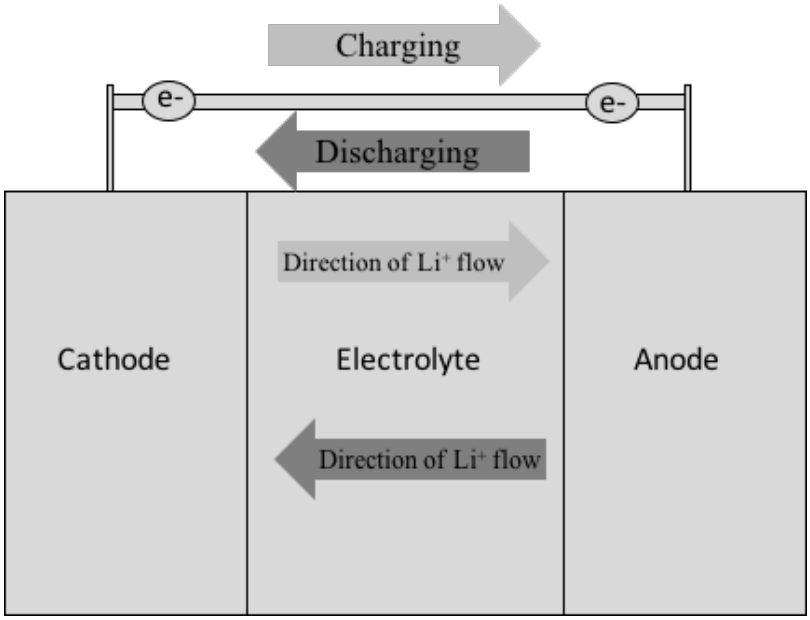

Figure 1-2: Schematic of lithium-ion battery. [Adapted from Reference 7].

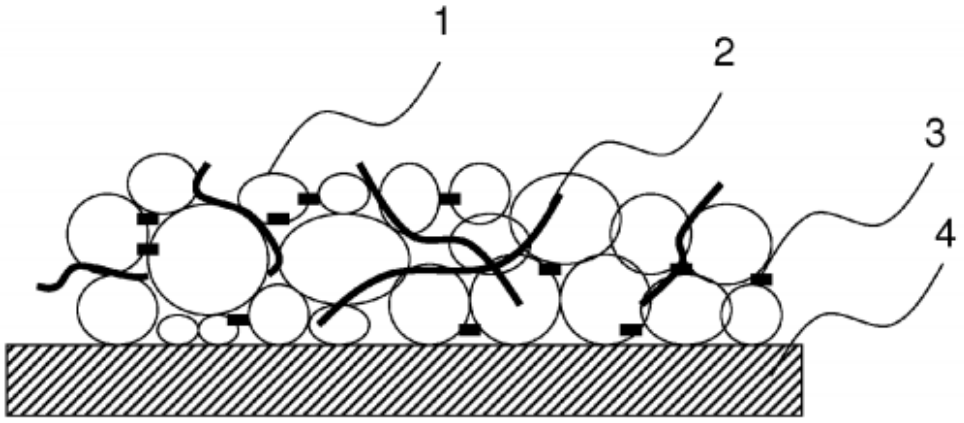

Figure 1-3: Schematic of electrode: (1) active material, (2) polymeric binder, (3) carbon additives, (4) current collector (Cu foil). [Reproduced with permission from the author[10]]

One of the major challenges for electrodes is to provide high capacity and high coulombic efficiency[11]. Graphite is widely used as a commercial anode material because of its high columbic efficiency and stable cycle performance, but it has a very low specific capacity[12]. To meet energy demands, electrode materials with higher energy and power densities are required[13]. Transition metal oxides (MO, where M is Co, Ni, Cu or Fe) are a promising alternative, due to their high theoretical capacity (~500-1000 mAh g^{-1})[14–17], but generally suffer from moderate coulombic efficiency[11]. The low coulombic efficiency results from a number of limitations, including the formation of the solid electrolyte interphase (SEI) film on the electrode surface and subsequent loss of electrical contact of the electrode with the current collector[11]. These shortcomings significantly reduce the effective *in operando* energy densities of Li-ion batteries. Thus, a common motif in battery design is developing a high capacity electrode without sacrificing long-term stability.

1.2 Magnetite as an Active Material

Magnetite (Fe_3O_4), which is particularly attractive, has a high theoretical capacity (~925 mAh g^{-1})[18], coupled with high electronic conductivity[18–20] and low cost; and it is environmentally friendly. Its high theoretical specific capacity results from the eight electron conversion reaction during the lithiation process[21], which is based on a novel conversion (Equation 1)[22].

$$Fe_3O_4 + 8Li^+ + 8e^- \rightleftarrows 3Fe^0 + 4Li_2O \quad (1)$$

However, just as most other transition metal oxides, Fe_3O_4 suffers from poor cycling performance, due to the large volume changes that take place during repetitive charging-discharging[23]. Magnetite has not been practically implemented as an anode material due its poor cyclic stability, resulting from drastic volume changes during insertion/de-insertion of Li-ion based on its conversion mechanism[24]. The drastic volume changes lead to electrical disconnection between the anode and current collector. Many strategies have been suggested to improve Fe_3O_4, including carbon coatings[25–27], nanostructures[28] and nanocomposites[13,22,24]. Carbon materials are often used to enhance electrical conductivity[29], improve rate performance[26] and have been shown to improve electrochemical properties of Fe_3O_4 anodes[25]. Carbon coatings improve cycling performance by acting as a buffer to relieve the volume changes occurring and therefore enhance electrochemical performance[24]. Carbon materials have previously been shown to be very stable anode materials, due to the small volume changes during Li insertion/extraction and that the SEI films on their surface are relatively stable[30–32].

Magnetite can be synthesized by various methods, including sol-gel[33], ultrasound irradiation[34], reverse micelle method[35], hydrothermal[36–38], thermal decomposition[37,39–48] and co-precipitation[29,48–52,52–57]. The most commonly used techniques are co-precipitation and thermal

decomposition. For this work, co-precipitation was used to synthesize magnetite with varied crystallite size and surface chemistries.

Co-precipitation is a desirable approach since it possible to do at low temperatures and does not require elaborate synthetic equipment[58]. However, co-precipitation does not provide as accurate control over particle size, compared to other techniques[59]. The technique typically involves mixtures of Fe^{2+} and Fe^{3+} dissolved in water and then base is added to form Fe_3O_4 precipitate[59]. Typical bases used are strong hydroxides, such as ammonium hydroxide[58].

1.3 PPBT/PEG System

Most electrode material research for Li-ion batteries focuses on the synthesis of active particles, with less emphasis on polymeric binders[60–63]. Recent studies[60–63] show the binder plays an essential role in stability and irreversible capacity loss, since the binder ensures electrode integrity during the volume changes in cycling. The most widely used polymeric binder, poly(vinylidene difluoride) (PVDF), attaches to the active material via weak van der Waals forces and fails to accommodate large changes in spacing between particles during cycling[62]. The role of active material-polymer interactions is vital for the electrode composition to enhance stability[63].

Recently, a poly[3-(potassium-4-butanoate)thiophene] (PPBT) binder component and a polyethylene glycol (PEG) surface coating for the active material was demonstrated to enhance both electron and ion transport in magnetite based anodes[2]. Electron pathway enhancement, such as through carbon coatings[2,39,41,64,65] is often considered in the design of battery anodes, but attention is rarely given to ion transport. PPBT is a water soluble, carboxylate substituted polythiophene. Conjugated polythiophenes have relatively high electronic conductivity, which enables electron transport[1]. In contrast, PVDF is insulating and further, requires the use of toxic

organic solvents[66]. As a water soluble binder, PPBT allows for more environmentally friendly electrode processing, while supporting pore formation for ion transport. Incorporation of PEG as a coating on the active material, reduces aggregate formation and improves active material dispersion leading to electron/ion transport enhancement[67]. The PEG/PPBT system is further investigated in this study as a facile approach to improve battery performance in Fe_3O_4 anodes.

While the PEG/PPBT system was shown to improve upon Fe_3O_4 based anode cycling performance[2], further performance enhancements are required for the design and development of robust Li-ion anode materials. Specifically, fundamental insight is needed into how active material surface chemistry and crystallite size impact battery performance. For instance, the synthesis method used for magnetite particle formation affects particle size, size distribution, agglomeration and surface chemistry[53]. Several synthetic methods have attempted to control crystallite size[36,38,59,68–70]; however, few studies attempt to explore the impact of changes in synthetic method on electrode performance, vis à vis electron and ion transport[53]. Further, while it has been suggested that the electrochemical activity of Fe_3O_4 depends on crystallite size[59,70], conclusions as to whether smaller or larger crystallites are optimal, remain elusive. This work explores how crystallite size and surface chemistry work in concert to impact Li-ion battery anode performance, thereby demonstrating the critical role of interfaces, coupled with electron and ion transport mechanisms, in the design of robust, high capacity electrode materials for battery applications.

CHAPTER 2 : MATERIALS AND METHODS

2.1 Materials

Fe_3O_4 nanoparticles (~10 nm and ~20 nm) were synthesized by previously reported coprecipitation processes, involving triethylamine base[59,70] or ammonium hydroxide base by collaborators at Stony Brook University. All 20 nm samples were synthesized using ammonium hydroxide, whereas 10 nm samples were synthesized with either triethylamine or ammonium hydroxide. For preparation of Fe_3O_4 particles coated with PEG (PEG-Fe_3O_4), 0.5 g of Fe_3O_4 powders in 5 g DI water were sonicated for 1.5 min at room temperature with an ultrasonic probe (3 pulses of 30 s each, operated at 50 W, Qsonica Q700 sonicator). Two mL of PEG 1500 solution (50% w/v, Sigma-Aldrich) was added with sonication for 30 s, and this process was repeated four times until the total amount of PEG 1500 added to the aqueous dispersion was 8 mL. The PEG-Fe_3O_4 powders were washed with acetone and extracted by centrifuge separation (VWR Clinical 200) with a speed of 6000 rpm for 5 min; this process was repeated 3 times. PPBT (M_w: 21 kDa, polydispersity: 2.2, head-to-tail regioregularity: 89%) was purchased from Rieke Metals Inc.

2.2 Methods

2.2.1 Electrode Fabrication and Electrochemistry

The slurries for the PPBT-based electrode were prepared by mixing of Fe_3O_4 (or PEG-Fe_3O_4) (0.214 g), carbon additives (0.043 g), and PPBT in DI water (10 wt % solution, 0.43 g), and in the case of the PVDF-based electrode, N-methyl-2-pyrrolidone (NMP) solvent was used (weight ratio of Fe_3O_4:carbon:polymer = 71.4:14.3:14.3). The electrodes for field-emission scanning electron microscopy (FE-SEM, Zeiss Ultra-60) measurement, energy dispersive x-ray

spectroscopy (EDS, Oxford Aztec software) measurement, electrochemical evaluation, and spectroscopy characterization were produced by blade coating (doctor blade, MTI corp). The PPBT-based electrodes were pre-evaporated at room temperature for 2 h and solvent was completely evaporated at 110°C for 12 h in a vacuum oven. In the case of the PVDF-based electrodes, the NMP solvent was pre-evaporated at 70°C for 1 h, and the other fabrication procedures remained the same as for the PPBT-based electrodes.

Half-cell stainless steel coin cells (Figure 2-1) were used for electrochemical measurements. Lithium metal, purchased from MTI corp., was used as a counter electrode and 1 M $LiPF_6$ in ethylene carbonate (EC) and diethylene carbonate (DEC) (1:1 by weight), purchased from BASF, was used as the electrolyte. Before electrochemical testing, the capacity of each coin cell was confirmed by charging and discharging at a current density of 40 mA g^{-1} (~0.05 C), using the Arbin battery cycler. Cycling and rate capability testing was then performed on the same Arbin battery cycler. Electrical impedance spectroscopy (EIS, Metrohm Autolab PGSTAT101) measurements were conducted in the frequency range from 0.1 MHz to 0.1 Hz.

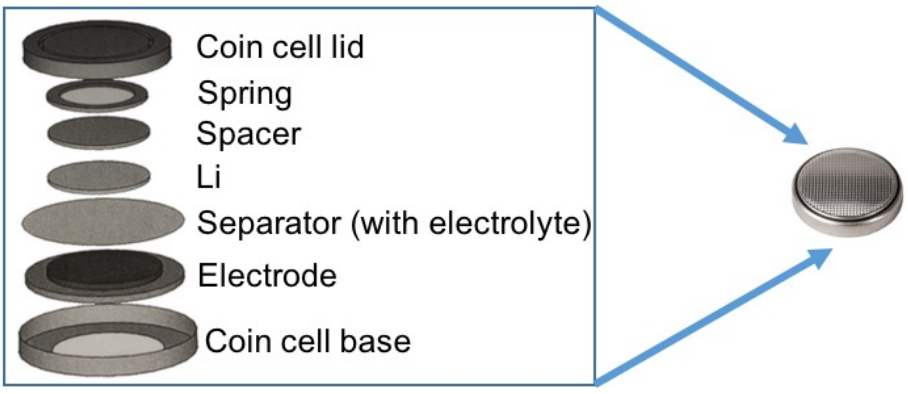

Figure 2-1: Coin cell schematic

2.2.2 Microscopic Characterization

FE-SEM images were observed on the surface view of the electrodes using the Zeiss Ultra-60 FE-SEM with an accelerating voltage of 5 kV using the high vacuum mode at room temperature. Element analysis was conducted using energy dispersive x-ray spectroscopy (EDS, Oxford Aztec software). Transmission electron microscopy (TEM) images were obtained using a Hitachi HT7700 TEM. First the Fe_3O_4 (or PEG-Fe_3O_4) powders were dispersed in ethanol and then the dispersion was drop-cast onto Formvar Film 200 Mesh Copper grids (Electron Microscopy Sciences) for subsequent TEM analysis.

2.2.3 Structure Characterization

X-ray powder diffraction patterns (XRD) of the products were obtained on a PANalytical Empyrean. Dynamic light scattering (DLS) and Zeta potential measurements were performed using a Malvern Zetasizer NANO ZS instrument (Malvern instruments). Fe_3O_4 (or PEG-Fe_3O_4) particles were dispersed in aqueous medium through bath-type sonication (Branson 2510) for 30 min (1 mg particles/1 mL deionized water). Thermogravimetric Analysis (TGA, TA Instruments Q600) was carried out in nitrogen in the temperature range of 25–600°C at a heating rate of 20°C/min.

2.2.4 Spectroscopic Characterization

The electrode samples for spectroscopic measurements were prepared by scraping powder samples from the prepared electrodes. Fourier transform infrared (FT-IR) spectra were recorded using KBr pellets of the materials using a Thermo Scientific Nicolet iS50 FT-IR spectrometer. X-ray spectroscopy (XPS) characterization was performed using a Thermo K-Alpha XPS system. The instrument was equipped with a monochromatic Al-K X-ray source

(1468 eV). Spectra were collected using the flood gun and an X-ray spot size of 400 μm. Survey scans were collected with pass energy of 200 eV with 1 eV increments. High resolution scans (for specific elements) were collected with pass energy of 50 eV with 0.1 eV increments.

CHAPTER 3 : ACTIVE MATERIAL CHARACTERIZATION

3.1 Introduction

The active materials used in this study, with different crystallite sizes and synthetic approaches, were characterized through XRD, TEM and DLS. First, the PEG-coating procedure is outlined, with emphasis given on how it reduces aggregates in Fe_3O_4. Before analyzing Fe_3O_4 (and PEG-Fe_3O_4) electrodes, initial characterization of the active material was done to confirm the magnetite phase and crystallite sizes. The magnetite (Fe_3O_4) phase was confirmed to ensure the samples synthesized by collaborators at Stony Brook were not maghemite or goethite, which are the most common impurity compounds when using the co-precipitation synthesis method[58]. The crystallite size was also verified, since one of the drawbacks associated with co-precipitation is less stringent control of crystallite size[59]. DLS characterizes colloidal stability[71], which provided aggregate size distribution and zeta potential for this work.

3.2 PEG-Coating

The propensity of magnetite nanoparticles to aggregate due to strong van der Waals and magnetic interactions is well known[72]. Introduction of polymers or organic molecules has been shown to stabilize the particles through both steric and electrostatic forces[39,65]. Polyethylene glycol (PEG) is perhaps one of the most frequently used polymers for such magnetite surface modification because it improves the colloidal stability of the particles. Thus, to reduce aggregate size and improve particle dispersion, PEG, which was shown previously to reduce aggregate size[2,64,65], was physically introduced onto the Fe_3O_4 particle surface. The procedure involved dispersion of Fe_3O_4 particles in a PEG 1500 containing aqueous medium via a probe-

type ultrasonication process[2,64]. Thermogravimetric analysis (TGA) confirmed the presence of ~12 wt % PEG (Figure 3-1).

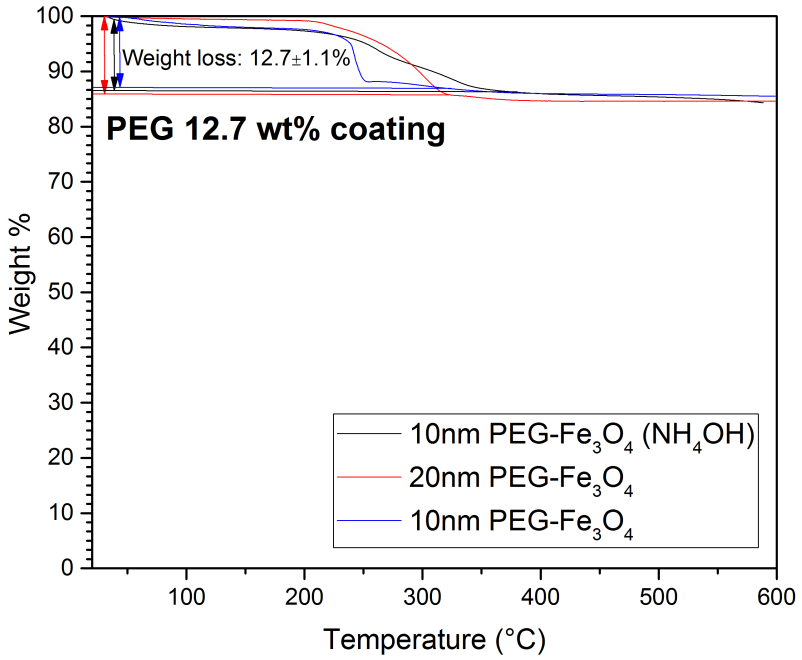

Figure 3-1: TGA profile of PEG coating, which is carried out in nitrogen in the temperature range of 25–600°C at a heating rate of 20°C/min, confirming ~12.7 wt% PEG coating.

3.3 Structure Characterization

Two different Fe_3O_4 crystallite sizes (~10 nm and ~20 nm), synthesized by a coprecipitation method, with either triethylamine and ammonium hydroxide as the base, were used in this investigation. As presented in Figure 3-2, XRD analysis confirmed that all samples were in the magnetite phase (Fe_3O_4) and the crystallite size was calculated using the (311) peak.

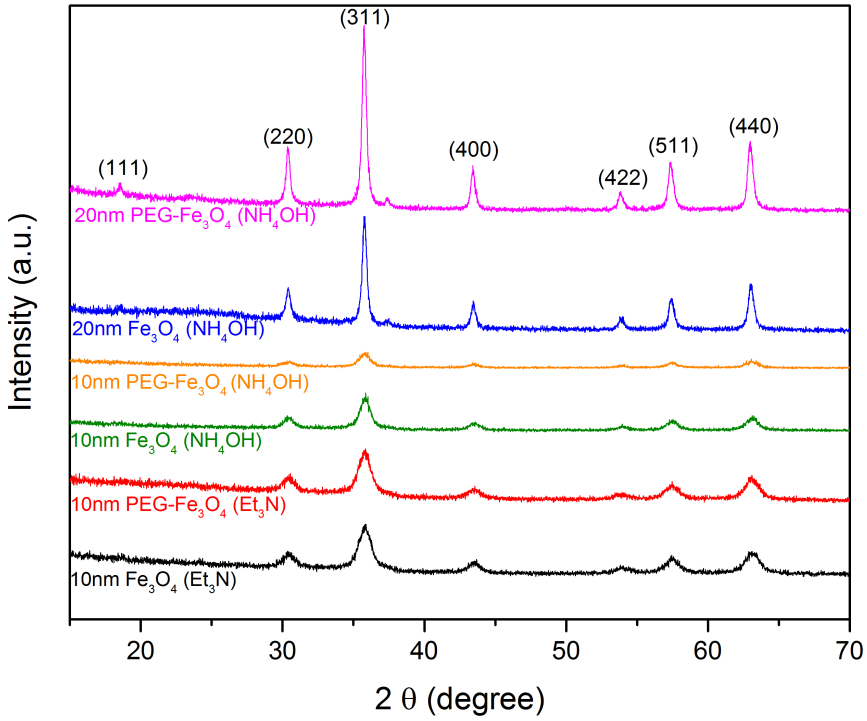

Figure 3-2: XRD patterns of Fe_3O_4 (or PEG-Fe_3O_4)

Crystallite size was corroborated through TEM image analysis (Figure 3-3), using ImageJ software (Figure 3-4). ImageJ measures the size of particles using its "set scale" function. First, the scale bar was measured to find the length in terms of pixels, which was used to set the scale bar length in nanometers (200 nm for all TEM images). Visible particles were then traced and measured, which could not be done for heavily aggregated particles. The results are summarized in Table 3-2.

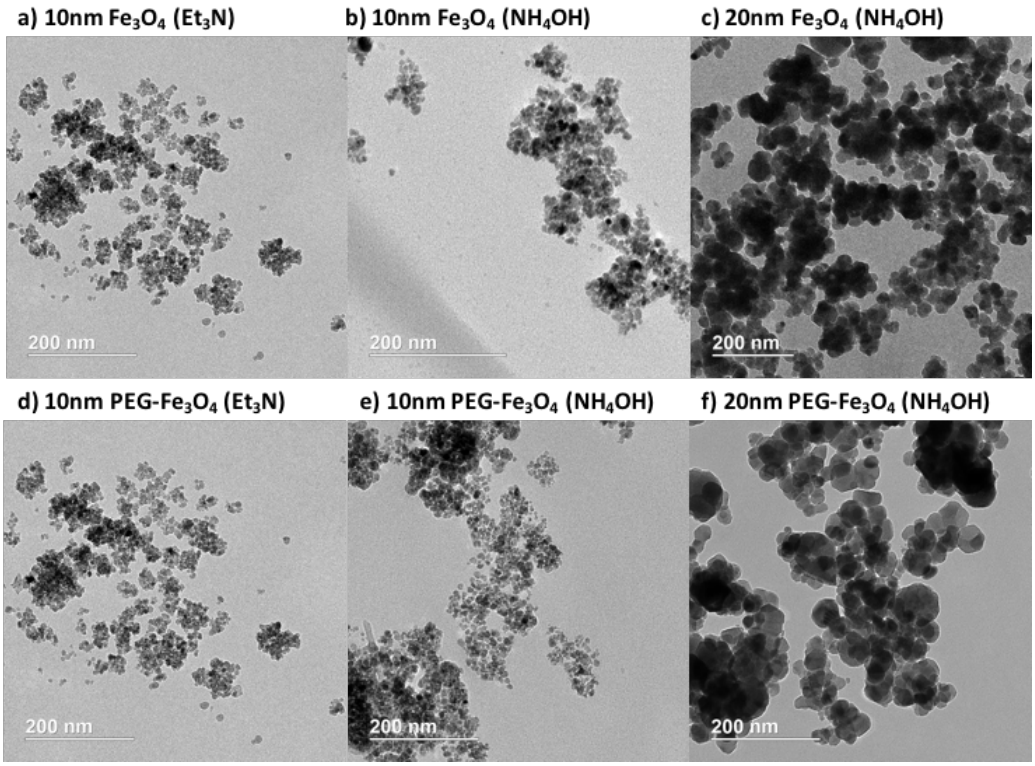

Figure 3-3: TEM images of Fe_3O_4 (or PEG-Fe_3O_4) dispersed in ethanol and drop-casted onto grids.

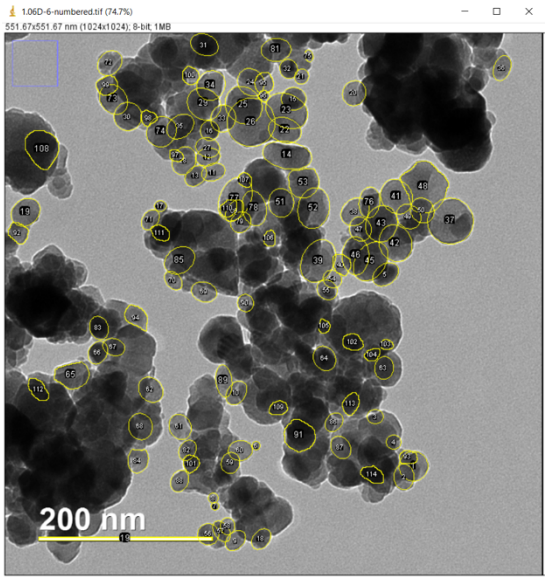

Figure 3-4: Example of ImageJ measurement technique.

Table 3-1: Crystallite Size (XRD and TEM).

Sample	Crystallite Size (XRD)	Crystallite Size (TEM)
10nm Fe_3O_4 (Et_3N)	6.11 nm	6.14 nm
10nm PEG-Fe_3O_4 (Et_3N)	7.32 nm	8.28 nm
10nm Fe_3O_4 (NH_4OH)	8.60 nm	7.59 nm
10nm PEG-Fe_3O_4 (NH_4OH)	8.89 nm	8.69 nm
20nm Fe_3O_4 (NH_4OH)	17.8 nm	18.79 nm
20nm PEG-Fe_3O_4 (NH_4OH)	22.0 nm	22.83 nm

3.4 Nanoparticle Stability

The extent to which the Fe_3O_4 and PEG-Fe_3O_4 powders formed aggregates during processing into electrodes was evaluated using dynamic light scattering (DLS). In efforts to mimic the immediate environment surrounding the nanoparticles, they were dispersed in water through a bath-type sonication process. The pristine Fe_3O_4 samples aggregated beyond the size limitations of the instrument and thus, aggregate size distribution could not be obtained. In the case of the PEG-Fe_3O_4 particles, DLS results (Figure 3-5, Table 3-2) demonstrated that there are two main aggregate sizes present in all PEG-coated samples.

Table 3-2: Aggregate size (DLS)

Sample	Average Aggregate Size (DLS)
10nm Fe_3O_4 (Et_3N)	--
10nm PEG-Fe_3O_4 (Et_3N)	312.3 nm
10nm Fe_3O_4 (NH_4OH)	--
10nm PEG-Fe_3O_4 (NH_4OH)	281.7 nm
20nm Fe_3O_4 (NH_4OH)	--
20nm PEG-Fe_3O_4 (NH_4OH)	215.6 nm

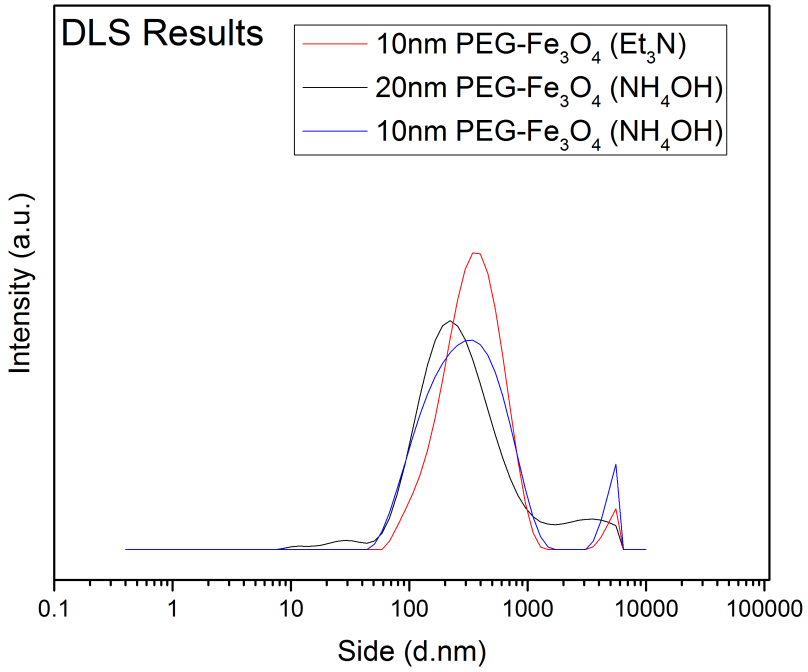

Figure 3-5: DLS results of PEG-Fe_3O_4 dispersed in DI water

Upon examination of the results presented in Table 3-2, two distinct differences between the samples are immediately apparent. First, the average aggregate size is larger for the 10 nm vs. 20 nm PEG-coated Fe_3O_4 nanoparticles, which were both prepared with ammonium hydroxide as the base. Second, and equally if not more insightful, is that the base used in the nanoparticle synthesis plays a role in determining aggregate size. Note that the average aggregate size for 10 nm crystallites prepared using trimethylamine is larger than that for the ammonium hydroxide counterparts, 310 vs. 280 nm, respectively. These results suggest that surface chemistry and by extension interfacial interactions may play a role in composite electrode performance.

Given previous reports that smaller particles tend to form larger aggregates in solution due to their larger surface to volume ratio[59], it was expected that the smaller crystallites would aggregate and form precipitates having larger average particle size in solution (Figure 3-5). The differences observed for particles having nominally the same crystallite size, but prepared using

an alternate base, namely, triethylamine or ammonium hydroxide, was not anticipated. In all cases examined here, the magnetite samples synthesized using ammonium hydroxide exhibited smaller average aggregate size compared to those derived from triethylamine after coating with PEG.

The Fe_3O_4 (or PEG-Fe_3O_4) powders were dispersed in water through bath-type sonication for zeta potential measurements to determine colloidal stability. Zeta potential is used to determine the surface charge of nanoparticles in solution and the magnitude helps predict colloidal stability[73]. Prior to zeta potential measurements, the pH of each solution was measured, with an average pH of 8.52 ± 0.6. For accurate zeta potential measurements, the pH should be consistent between samples, which is mostly true here.

Table 3-3: Zeta Potential Values for Fe_3O_4 and PEG-Fe_3O_4 samples dispersed in water

Sample	Zeta Potential (mV)	pH
10nm Fe_3O_4 (NH_4OH)	-36.50 ± 0.95	9.6
10nm PEG-Fe_3O_4 (NH_4OH)	-32.13 ± 1.32	8.88
20nm Fe_3O_4 (NH_4OH)	-37.60 ± 0.36	8.53
20nm PEG-Fe_3O_4 (NH_4OH)	-31.77 ± 0.32	8.35
10nm Fe_3O_4 (Et_3N)	-34.63 ± 1.07	8.06
10nm PEG-Fe_3O_4 (Et_3N)	-34.23 ± 1.26	8.01

The zeta potential value ± 25mV is used as the baseline of high stability for solutions. All the samples here (Table 3-3) are below –25mV, which indicates a degree of stability. The more negative a value of zeta potential, the more stable the sample is. Here, it would be expected that the PEG-coated samples would have higher stability, since PEG has been shown to reduce aggregates. Due to shielding caused by the PEG-coating, the PEG samples have a lower zeta potential value. These zeta potential values provide preliminary indication that the uncoated ammonium hydroxide samples (10 nm and 20 nm) have higher stability compared to the triethylamine sample (10 nm). Perhaps more significant, with the PEG-coating, it appears the

triethylamine sample (10 nm) has higher stability compared to the ammonium hydroxide samples (10 nm and 20 nm). These zeta potential results provide preliminary insight into the stability of the system to be discussed.

3.5 Conclusion

XRD confirmed all samples were in the magnetite phase and in conjunction with TEM verified the crystallite sizes (~10 nm and 20 nm). DLS and zeta potential results provide early insight into the differences between synthetic approaches, i.e. triethylamine vs. ammonium hydroxide. The differences in aggregate size favor the ammonium hydroxide system, whereas zeta potential indicates the triethylamine PEG-coated samples could be more stable. Further information on morphology, electrochemical characterization and chemical characterization are provided in forthcoming chapters to explain the differences in crystallite size and surface chemistry.

CHAPTER 4 : EFFECT OF ACTIVE MATERIAL SURFACE CHEMISTRY ON THE PERFORMANCE OF Fe_3O_4 Li-ION BATTERY ANODES

4.1 Introduction

Controlling the morphology and structure has been shown to influence the performance of transition metal oxides[21]. Specifically, magnetite of various morphologies has been synthesized to achieve better performance[25,37]. Of the different morphologies, hollow spheres have been shown to achieve the highest capacity and capacity retention over 50 cycles[29,43]. The hollow sphere morphology is able to alleviate the stress from volume changes during cycling[43,74,75]. Magnetite nanoparticles with different shapes including octahedral[76] and hexahedra[77] have also shown improved performance. Manipulation of morphology improves and alters electrochemical performance.

For this work, co-precipitation was used to synthesize magnetite with varied surface chemistries, using ammonium hydroxide or triethylamine bases, to compare morphology differences. Alkyl amines provide pH control, hence triethylamine was used here for its low volatility and ability to form a buffer in aqueous solution[59]. Alternatively, ammonium hydroxide is the most frequently used base for synthesis and was used for comparison. However, this method requires careful maintenance of Fe^{2+}:Fe^{3+} ion ratio in 1:2 and adjustment of pH[58].

Several magnetite synthesis methods have been previously described, mainly to provide crystallite size control[36,38,59,68–70], but few studies exist to describe the effect of different bases[53]. Mascolo *et al*. studied NaOH, KOH and $(C_2H_5)_4NOH$ bases for the co-precipitation synthesis method and how they affected the formation of mesoporous structures, specifically looking at magnetite for medical applications. This study indicated particle size decreases according to the

cation size of the base in the following manner: $Na^+ > K^+ > N(C_2H_4)^+$, which was attributed to the effects of steric hindrance hampering agglomeration among individual particles[53].

Although many studies discuss morphological effects of magnetite, there is a gap in the literature to address differences in synthetic approaches on magnetite properties for electrochemical performance. This section addresses how the triethylamine and ammonium hydroxide synthesis techniques impact electrochemical performance.

4.2 Results and Discussion

4.2.1 Microscopic Characterization

The impact of the observed aggregation behavior of the particles on electrode physical and chemical characteristics, and electrode performance was examined through fabrication of magnetite based electrodes via standard procedures: Fe_3O_4 or PEG-Fe_3O_4, carbon additives and poly[3-(potassium-4-butanoate)thiophene] (PPBT) polymeric binder were mixed in the usual manner, the resulting slurry was blade coated onto a Cu foil current collector, and then dried. Control electrodes were also fabricated using the more commonly used binder, poly(vinylidene difluoride) (PVDF)[66]. Electrode morphology was investigated using field-emission scanning electron microscopy (FE-SEM) to determine the level of materials dispersion within the processed composites (Figure 4-1). EDS SEM imaging and elemental (Fe, O, C) image mapping (Figure 4-2) confirmed the presence of Fe_3O_4 nanoparticles, carbon additives, and PPBT binder in all fabricated electrodes.

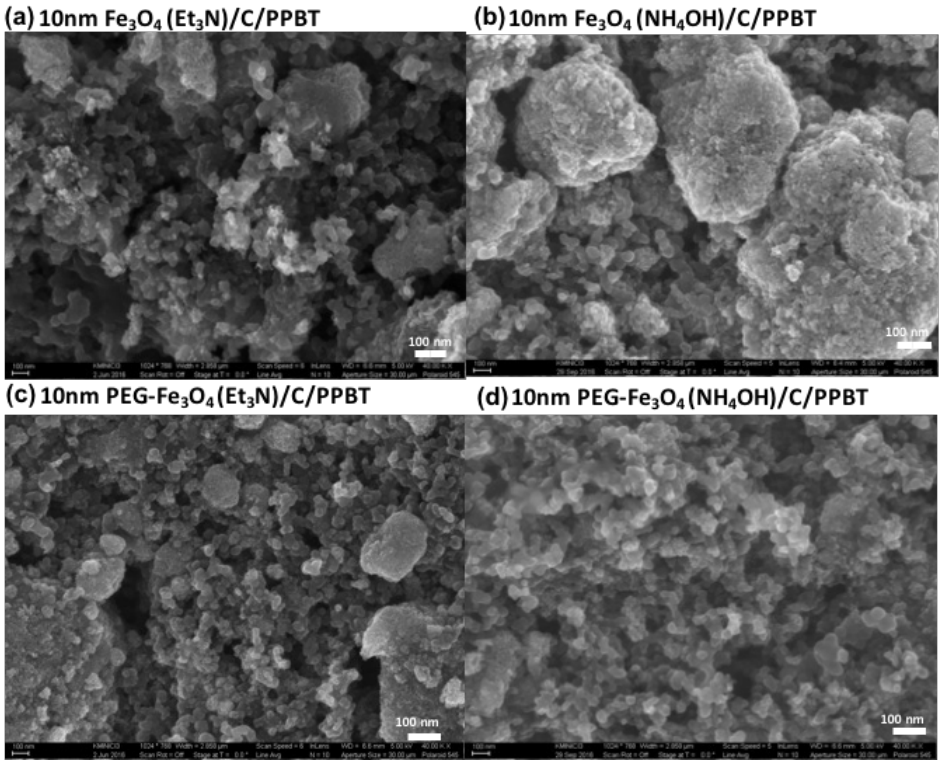

Figure 4-1: FE-SEM of top view electrodes.

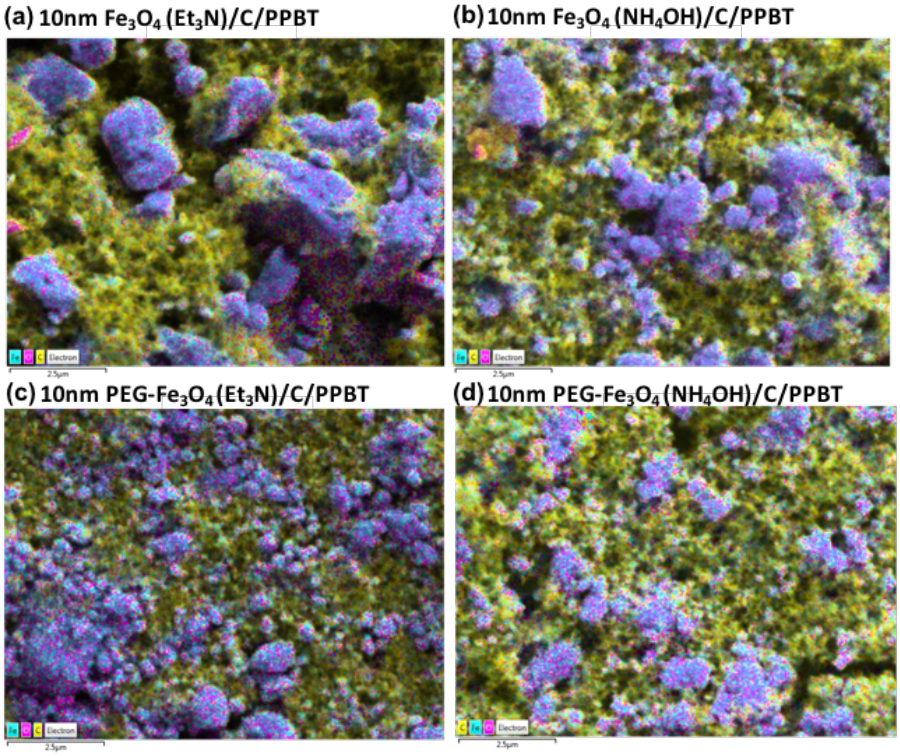

Figure 4-2: EDS SEM image maps of electrodes (top view) with blue corresponding to iron, yellow corresponding to carbon and pink corresponding to oxygen in electrodes.

As anticipated from previous reports and DLS characterization, introduction of the PEG-coating onto the Fe_3O_4 nanoparticles led to a reduction in aggregate size within the composite electrode[2]. For all active material particle sizes and synthesis procedures, incorporation of the PEG-coating appeared to decrease aggregation and afford a composite electrode with more uniformly dispersed components, which is generally expected to enhance battery performance[2]. Note that the uncoated 10 nm (triethylamine) based electrodes vs. those that were PEG-coated exhibited smaller aggregates (Figure 4-1a, c), as was also observed for the 10 nm ammonium hydroxide derived electrode (Figure 4-1b, d).

Closer examination of the images presented in Figure 4-1 do, however, exhibit some distinct differences. For instance, the electrodes synthesized with triethylamine (Figure 4-1a, c) are not as well-dispersed, even with the PEG-coating (Figure 4-1c). While it has been suggested that a reduction in the aggregate size should lead to improved electron and ion transport[2], an overly uniform morphology might also impede the electron transport process required for effective performance and hinder the transport pathways.

The morphological differences between the triethylamine and ammonium hydroxide synthesis methods were further investigated by FE-SEM imaging of electrodes fabricated with the control PVDF binder (Figure 4-3). In comparison to PPBT, the use of PVDF results in the formation of noticeably larger aggregates (Figure 4-3 insets). Further, the use of ammonium hydroxide in the active material synthesis leads to more well-dispersed composites in the case of PVDF (Figure 4-3b), though the level of dispersion is not as extensive as was observed with PPBT.

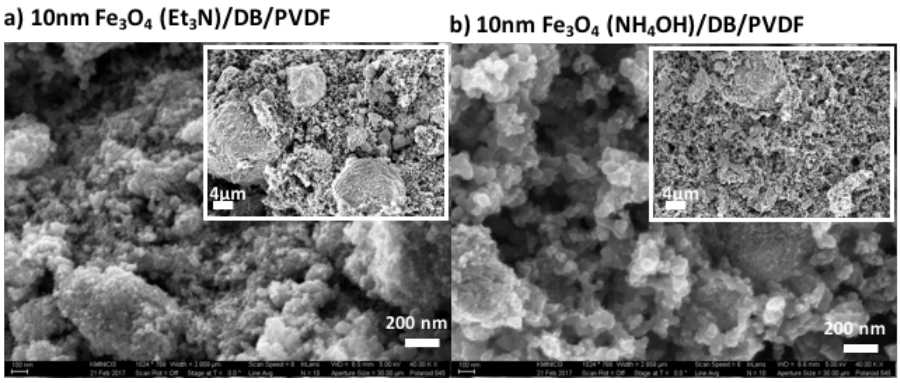

Figure 4-3: FE-SEM top view images of PVDF control electrodes.

4.2.2. Electrochemistry

From an electrochemical performance perspective, coin cells with a Li metal counter electrode were utilized and all the electrodes were prepared with Fe_3O_4 (or PEG-Fe_3O_4) active material, carbon additives, and polymeric binder in a 71.4:14.3:14.3 mass ratio. The mass ratio was chosen because in a previous study[1], the electrode exhibited its percolation threshold in electronic conductivity at this ratio. The electrolyte was 1 M $LiPF_6$ in ethylene carbonate (EC) and diethylene carbonate (DEC) (1:1 by weight).

Charging-discharging cycling (Figure 4-4) was conducted at a current density of 240 mA g^{-1} (~0.3 C) to determine capacity retention of the electrodes. The benefits of the PEG/PPBT system are apparent for electrodes fabricated from the alternative synthetic chemistries, where the PEG-coating significantly enhanced cycling performance. Initial charge capacity (Table 4-1) does not provide meaningful differences between synthetic approaches and coated vs. uncoated electrodes. More important differences stem from the effect of the synthetic approaches on capacity retention.

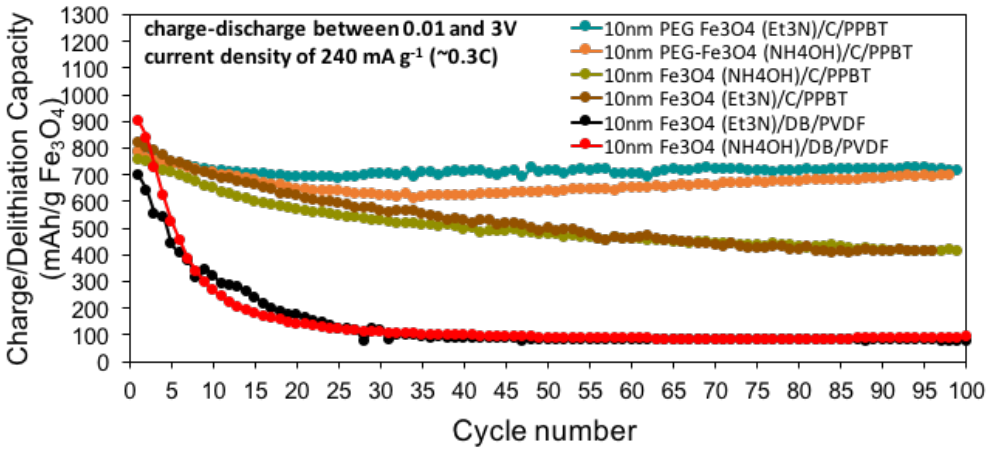

Figure 4-4: Cycling performance (capacity retention as a function of cycle number) collected for current density of 240 mA g-1 (~0.3C) between 0.01 and 3V

Table 4-1: Initial discharge capacity values and capacity retention during cycling.

Electrode	Initial Charge/Delithiation Capacity (Figure 4-4)	Capacity Retention (%) After 100 Cycles (Figure 4-4)
10 nm Fe_3O_4 (Et_3N)/PPBT	820 mAh/g Fe_3O_4	50 %
10 nm PEG-Fe_3O_4 (Et_3N)/PPBT	790 mAh/g Fe_3O_4	91 %
10 nm Fe_3O_4 (NH_4OH)/PPBT	750 mAh/g Fe_3O_4	54 %
10 nm PEG-Fe_3O_4 (NH_4OH)/PPBT	790 mAh/g Fe_3O_4	89 %
10 nm Fe_3O_4 (Et_3N)/DB/PVDF	698 mAh/g Fe_3O_4	11 %
10 nm Fe_3O_4 (NH_4OH)/DB/PVDF	900 mAh/g Fe_3O_4	10 %

Investigating the impact of synthetic chemistries on capacity retention, the triethylamine base (teal line) maintained a higher capacity over 100 cycles compared to the ammonium hydroxide base (orange line). Cycling performance further indicates the overly dispersed morphology seen in the ammonium hydroxide base could be worse for electron and ion transport.

Comparing synthetic approaches within the PVDF electrodes effect on cycling performance (Figure 4-4), the 10 nm (ammonium hydroxide)/PVDF electrode (red line) had a higher initial capacity compared to the 10 nm (triethylamine)/PVDF electrode (black line). This difference between synthetic chemistries could be a result of the morphology differences seen in

FE-SEM (Figure 4-3) – recall the ammonium hydroxide/PVDF electrodes are more dispersed and exhibit less aggregate formation than the triethylamine/PVDF electrodes. Here, the large aggregates present in the triethylamine synthetic approach appear to hinder electron/ion transport.

To further investigate battery performance, newly fabricated half cells were subjected to rate capability experiments (Figure 4-5), where cells were lithiated at a constant current density of 80 mA g^{-1} (~0.1C) and delithiated over a wide range of current densities (80 – 1600 mA g^{-1}) at a voltage range of 0.01 – 3 V. Overall, the PEG-Fe_3O_4/PPBT binder-based electrodes show much higher delithiated capacity than the PVDF control, which conveys its superior rate capability. Through rate capability testing, the 10 nm (ammonium hydroxide)/PPBT electrode displayed higher capacity vs. the 10 nm (triethylamine)/PPBT electrode (teal line), particularly at higher current densities, while both exhibited similar capacity retention. The rate capability performance differences are best attributed to the morphological differences (Figure 4-1). The more dispersed ammonium hydroxide derived electrodes could prove better for rate capability testing, as demonstrated at higher current densities. However, EIS analysis and spectroscopic characterization provide further insight into the observed differences in performance for nanoparticles prepared via the triethylamine and ammonium hydroxide routes, and shed light as to the impact of surface chemistry and interfacial interactions between the individual components of the anode.

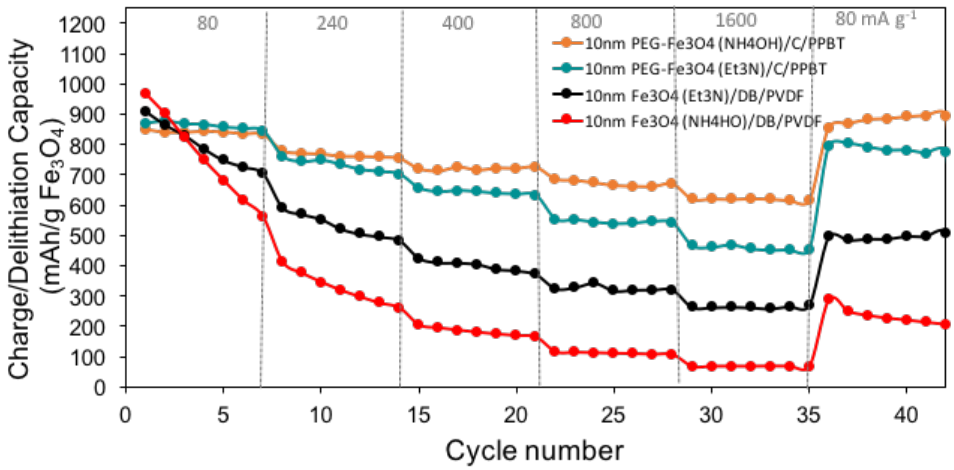

Figure 4-5: Delithiation rate capability, where cells were lithiated at a constant current density of 80 mA g^{-1} and delithiated at different current densities between 0.01 and 3V

EIS analysis presented in Figure 4-6 supports the cycling (Figure 4-4) and rate capability (Figure 4-5) data. The cells used in the EIS study correspond to those cycled between 0.01 and 3V as shown in Figure 4-4. Impedance testing was performed in the frequency range of 0.1 MHz to 0.1 Hz before cycling at 3V and after 100 cycles at their open-circuit voltage (OCV). Superior battery electrode performance can be attributed to decreased charge transfer resistance (R_{ct}), which is estimated from the diameter of the semicircle[78]. Initially, the charge transfer resistance was not effectively reduced in the PEG-PPBT vs. PVDF control system (Figure 4-6a).

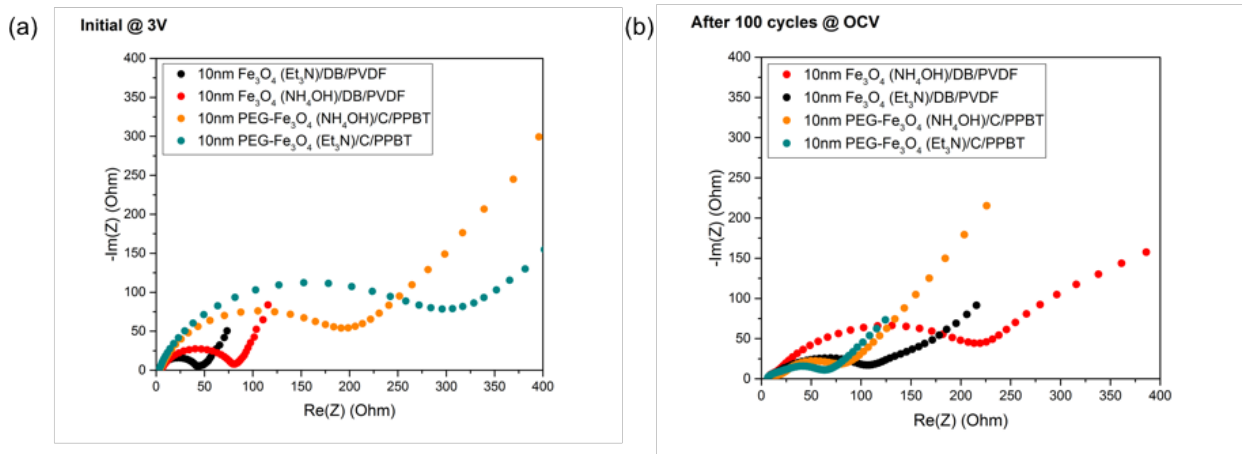

Figure 4-6: (a) Impedance spectra measured at 3V before cycling in the frequency range from 0.1 MHz to 0.1 Hz (b) Impedance spectra measured at open-circuit voltage (OCV) after 100 cycles in the frequency range from 0.1 MHz to 0.1 Hz

After 100 cycles (Figure 4-6b), the positive effects of introducing PEG/PPBT are clearly noticeable for the 'ammonium hydroxide' electrodes, where the charge transfer resistance decreased significantly, compared to the PVDF electrodes. More importantly, using 10 nm magnetite crystallites synthesized with triethylamine in conjunction with PPBT (teal semicircle) afforded still lower charge transfer resistance, which further supports the advantages of one synthetic approach over the other, and the resultant impact on surface interactions and ultimate performance characteristics of high capacity composite electrodes. Note that the triethylamine derived active material (black semicircle) exhibited comparable, but larger, charge transfer resistance to the ammonium hydroxide/PPBT system (orange semicircles) after 100 cycles, even when PVDF was used as the binder.

4.2.3. Spectroscopic Characterization

Both electron and ion transport are known to be aided through molecular interactions between PPBT and Fe_3O_4 or PEG-Fe_3O_4[2]. Here, Fourier transform infrared (FT-IR) spectroscopy

confirmed that PEG effectively interacts with and modifies the surface of Fe_3O_4 regardless of synthetic approach (Figure 4-7).

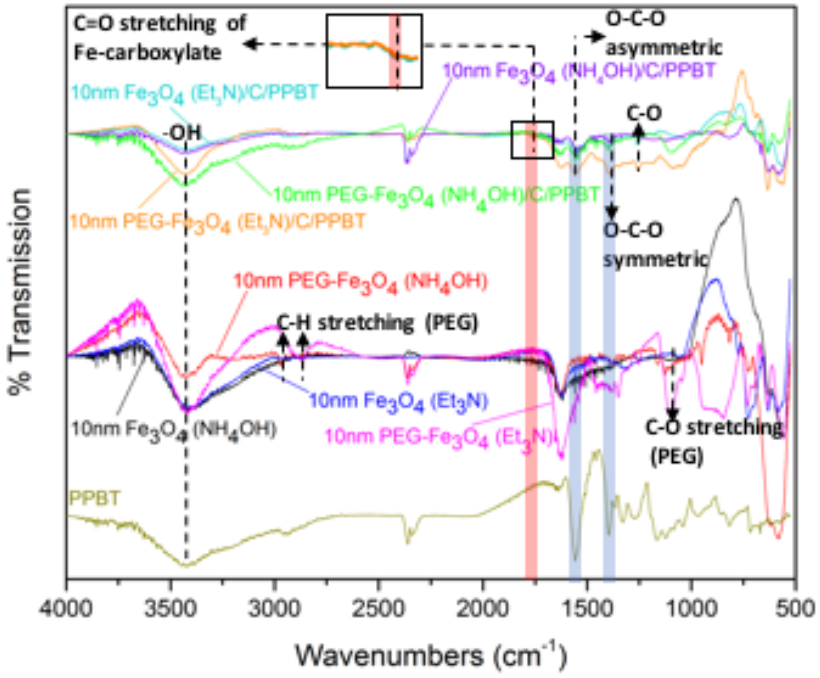

Figure 4-7: FT-IR spectra of materials (bottom lines: PPBT, Fe_3O_4, PEG-Fe_3O_4) and electrodes (upper lines: Fe_3O_4/C/PPBT, PEG- Fe_3O_4/C/PPBT).

Sharp C-H and C-O stretching bands at 2875 cm^{-1} and 1125 cm^{-1}, respectively, confirmed Fe_3O_4 surface modification with PEG[67]. FT-IR was further used to interrogate the chemical interactions within the composite electrodes. This was accomplished by first blending the requisite components, fabricating the electrodes and then scraping the resultant system to retrieve the powder material. All PPBT-based electrodes fabricated with all Fe_3O_4 and PEG-Fe_3O_4 samples, exhibited the stretching bands associated with the binder, PPBT; specifically, the carboxylate anion O-C-O asymmetric and symmetric stretching bands were observed at 1550 cm^{-1} and 1400 cm^{-1}, respectively[60,61,79,80] (Figure 4-7).

In addition to these peaks, a lower intensity vibration (Figure 4-7 inset) that was seen only for the trimethylamine based Fe_3O_4 and PEG-Fe_3O_4 electrodes (orange and cyan lines), was observed at 1760 cm^{-1}. Based on the peak position, this band is suggested to correspond to a Fe-carboxylate interaction[2]. Although the peak intensity is low, neither PPBT nor Fe_3O_4 exhibit a vibration at this position, and thus this band points to chemical interactions between PPBT and Fe_3O_4 within the composite electrode. Such interactions are considered to be a critical factor for electrode stability[60–63], yet prior to the introduction of PPBT as an alternative binder, interactions between active material and binder had only been reported for Si-based anodes. Figure 4-8 presents a structural representation of the proposed Fe_3O_4-PPBT chemical interactions, which helps illustrate the effects on the C=O and O-C-O FTIR stretching bands[2,81].

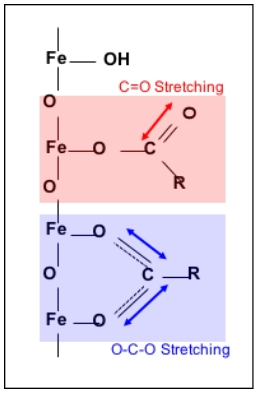

Figure 4-8: Proposed chemical structure of Fe_3O_4 in the electrode.[2]

The 1760 cm^{-1} vibration is not as clearly visible in the spectrum of electrode composites fabricated with the ammonium hydroxide derived magnetite. While the O-C-O asymmetric and stretching bands (Figure 4-7) are observed, the additional proposed Fe-carboxylate vibration is not present. Thus, the vibrational spectroscopy results suggest that the active material synthetic method is likely to impact the surface chemistry of the resultant materials and as a consequence both bonding and non-bonding interactions between composite electrode components. These

interactions may further play a significant role in determining electrode stability, a key factor that impacts battery performance. Recall that when the active material was synthesized with triethylamine, the electrode exhibited better capacity retention over 100 cycles in comparison to the ammonium hydroxide alternative (Figure 4-4). These results serve to emphasize the crucial role of surface chemistry and by extension, interfacial interactions on the performance of Fe_3O_4-anode systems. In the case of ammonium hydroxide, it is conceivable that the PPBT binder can interact with residual base residing on the surface of the nanoparticles, which might explain why the previously described Fe_3O_4-PPBT interactions were not observed in the FTIR spectra of the ammonium hydroxide based electrodes (Figure 4-7).

XPS spectra of the C1s core level (Figure 4-9) further indicate the presence of chemical interactions. The bottom lines are spectra from the PEG-Fe_3O_4 powders of all samples, which exhibit a C-OH bond further confirming PEG surface modification to Fe_3O_4 particles[82]. The first peak at ~285eV, exhibited in all PPBT-based electrodes, corresponds to the C-O bond[83]. The next peak at ~287eV is associated to the carboxylate (COO-) bond. The chemical shifts to a lower binding energy indicate an increase in interatomic distance, which could result from the additional bonding between PPBT and Fe_3O_4[84]. The remaining two peaks in the XPS spectra are associated to satellite peaks, which often result from extended delocalized electrons in a sample and provide evidence to π-π^* interchain stacking along the PPBT backbone[85]. Such π-π^* stacking may induce intermolecular charge transport, which leads to improved electrical properties of the PPBT binder system[2].

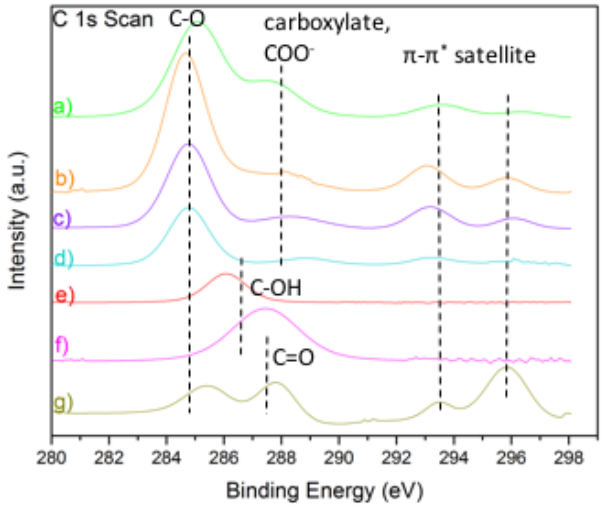

Figure 4-9: XPS spectra of C1s scan. (a) 10nm PEG-Fe_3O_4 (NH_4OH)/C/PPBT, (b) 10nm PEG-Fe_3O_4 (Et_3N)/C/PPBT, (c) 10nm Fe_3O_4 (NH_4OH)/C/PPBT, (d) 10nm Fe_3O_4 (Et_3N)/C/PPBT, (e) 10nm PEG-Fe_3O_4 (NH_4OH), (f) 10nm PEG-Fe_3O_4 (Et_3N), (g) PPBT

XPS spectra of Fe 2p core level (Figure 4-10) provides additional information about the magnetite phase present in the parent materials and electrodes. The first peak at ~712 eV corresponds to the Fe $2p_{3/2}$ core level electrons and the final peak at ~724 eV corresponds to the Fe $2p_{1/2}$ core levels[86]. The remaining middle peak corresponds to Fe^{3+}, which when absent, confirms a pure magnetite phase[82]. The presence of this peak would be further indication of chemical interaction between PPBT carboxylic moieties and the Fe_3O_4 surface, which is seen in the PEG-coated triethylamine derived electrode (Figure 4-10b, orange line). Hence, the Fe 2p scan provides further evidence to the chemical interactions between Fe_3O_4 and PPBT in the triethylamine synthesized electrodes. The lack of this satellite peak in the ammonium hydroxide electrodes further suggests they do not exhibit the chemical interactions indicative of electrode stability.

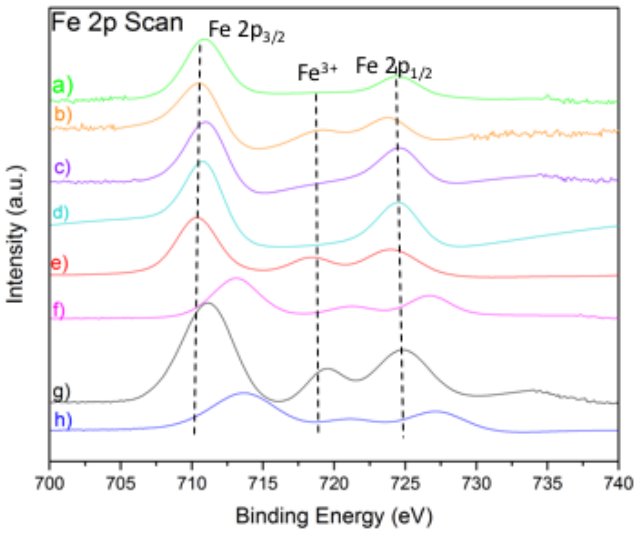

Figure 4-10: XPS spectra of Fe 2p scan. (a) 10nm PEG-Fe_3O_4 (NH_4OH)/C/PPBT, (b) 10nm PEG-Fe_3O_4 (Et_3N)/C/PPBT, (c) 10nm Fe_3O_4 (NH_4OH)/C/PPBT, (d) 10nm Fe_3O_4 (Et_3N)/C/PPBT, (e) 10nm PEG-Fe_3O_4 (NH_4OH), (f) 10nm PEG-Fe_3O_4 (Et_3N), (g) 10nm Fe_3O_4 (NH_4OH), (h) 10nm Fe_3O_4 (Et_3N)

4.3 Conclusion

Surface chemistry plays a crucial role in active material synthesis and influences interactions, as was demonstrated by the differences in triethylamine and ammonium hydroxide. The different synthetic approaches provided different environments for the electrode system, which did not result in the same chemical interactions. The nature and strengths of chemical bonding between binder and active material surface have previously been shown to influence electrochemical performance[63]. As described above, the triethylamine allows for interfacial interactions between the active material and binder that are essential for electrode stability. Whereas, these interactions are not visibly present in the ammonium hydroxide derived electrodes. Differences in interactions could provide further insight into the superior electrochemical performance of the triethylamine system, as exhibited in capacity retention and decreased charge transfer resistance. Furthermore, morphological differences between both

surface chemistries could explain why the ammonium hydroxide derived electrodes resulted in superior rate capability performance. Further insight into different surface chemistries and their effect on battery performance is needed for a fundamental understanding of their role in electrode fabrication towards robust high capacity Li-ion battery anodes.

CHAPTER 5 : EFFECT OF ACTIVE MATERIAL CRYSTALLITE SIZE ON THE PERFORMANCE OF Fe_3O_4 Li-ION BATTERY ANODES

5.1 Introduction

In previous studies, researchers studied factors that would affect crystallite size, such as pH[87,88], stir rate[52] and temperature[88,89]. The first investigation into the crystallite size effect for Fe_3O_4 was conducted by Komaba and coworkers[90], where they studied 400, 100 and 10 nm magnetite. Since the magnetite used in this study was not synthesized with a uniform technique, a clear analysis of crystallite size trends cannot be determined. However, they concluded that electrochemical activity is size dependent and that nanocrystalline (10 nm) Fe_3O_4 had the highest initial capacity.

Sizing down particles to the nanoscale has been shown to shorten the Li^+ diffusion pathway and increase reversible capacity and rate capability[1,21,29]. The first report of nanosized transition metal oxide electrodes exhibited reversible capacities up to three times higher than graphite[91]. However, nanoparticle-based electrodes have a higher propensity to aggregate because of van der Waals interparticle attractions[69]. Aggregation disrupts conductive pathways and can contribute to increased charge resistance in the electrode. Another challenge at the active material nanoscale includes undesirable side reactions with electrolyte, due to the large surface area[8,29]. To compensate for these surface area issues, stabilizing agents are attached to the surface of the particle to provide spatial insolation[69]. Furthermore, the large surface area/volume ratios provide more pathways for ion movement. The smaller size also improves kinetics in the electrode, since the Li^+ ion diffusion path occurs along smaller distances[29].

Following Komaba and coworkers' study, the Takeuchi group further investigated crystallite size effects, using Fe_3O_4 synthesized with the same technique (co-precipitation) and

base (triethylamine)[59,70]. In their first crystallite size control study[70], a direct evaluation of crystallite size on electrochemical performance was reported. This was the first study where all Fe_3O_4 samples were prepared by the same technique to investigate electrochemistry. Their findings demonstrated that the capacity was higher for smaller crystallite size (6 nm vs. 10 nm), but no information was provided on capacity retention or rate capability. There is also a margin of error associated with each crystallite size, since one of the drawbacks associated with the co-precipitation synthesis method is less rigorous control of crystallite size[59].

In the Takeuchi group's next crystallite size control study[59], concentration of triethylamine provided size control, by keeping temperature, stir rate and pH constant. Again, it was determined that the smaller crystallite size (6 nm vs. 10 nm) had a higher capacity, but no other electrochemical information was reported. Despite these studies, there is not a clear indication of whether smaller or larger crystallite size is preferential. This section addresses how different crystallite sizes (10 nm vs. 20 nm) impact electrochemical performance.

5.2 Results and Discussion

5.2.1 Microscopic Characterization

The impact of the observed aggregation behavior of the particles on electrode physical and chemical characteristics, and electrode performance was examined through fabrication of magnetite based electrodes via standard procedures: Fe_3O_4 or PEG-Fe_3O_4, carbon additives and PPBT polymeric binder were mixed in the usual manner, the resulting slurry was blade coated onto a Cu foil current collector, and then dried. Control electrodes were also fabricated using the more commonly used binder, PVDF[66]. Electrode morphology was investigated using FE-SEM to determine the level of materials dispersion within the processed composites (Figure 5-1). EDS

SEM imaging and elemental (Fe, O, C) image mapping (Figure 5-2) confirmed the presence of Fe_3O_4 nanoparticles, carbon additives, and PPBT binder in all fabricated electrodes.

As anticipated from previous reports and DLS characterization, introduction of the PEG-coating onto the Fe_3O_4 nanoparticles led to a reduction in aggregate size within the composite[2]. For all active material particle sizes, incorporation of the PEG-coating appeared to decrease aggregation and afford a composite electrode with more uniformly dispersed components, which is generally expected to enhance battery performance[2]. Note that the uncoated electrodes vs. those that were PEG-coated exhibited smaller aggregates for the 20 nm (Figure 5-1a, c) and 10 nm (Figure 5-1b, d) ammonium hydroxide derived electrodes. Electrodes fabricated with magnetite synthesized using the ammonium hydroxide route and then treated with PEG (PEG-Fe_3O_4) (Figure 5-1c, d) exhibited essentially identical morphology, despite differences in active material particle size.

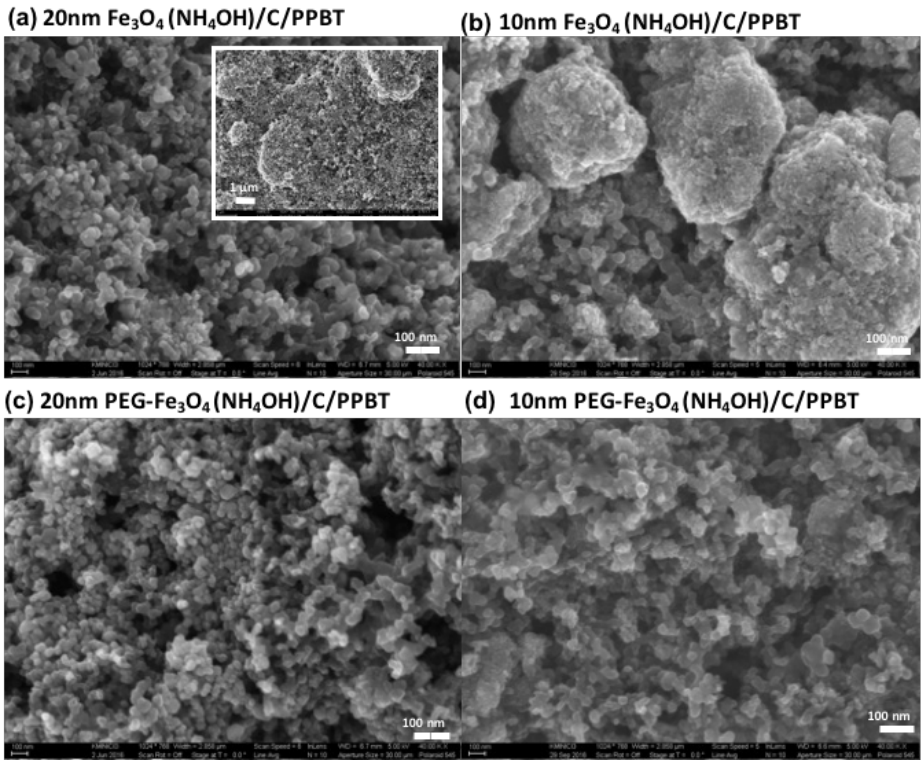

Figure 5-1: FE-SEM of top view electrodes.

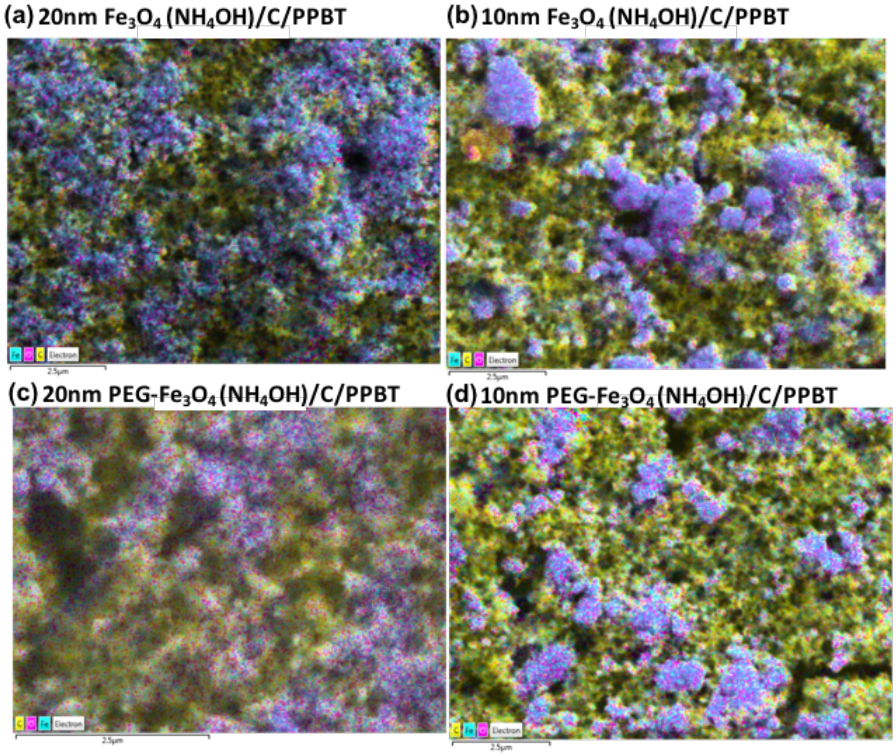

Figure 5-2: EDS SEM image maps of electrodes (top view) with blue corresponding to iron, yellow corresponding to carbon and pink corresponding to oxygen in electrodes.

The morphological differences between active material sizes was further investigated by FE-SEM imaging of electrodes fabricated with the control PVDF binder (Figure 5-3). In comparison to PPBT, the use of PVDF results in the formation of noticeably larger aggregates (Figure 5-3insets). Further, use of ammonium hydroxide in the active material synthesis leads to well-dispersed composites in the case of PVDF, though the level of dispersion is not as extensive as is observed with PPBT.

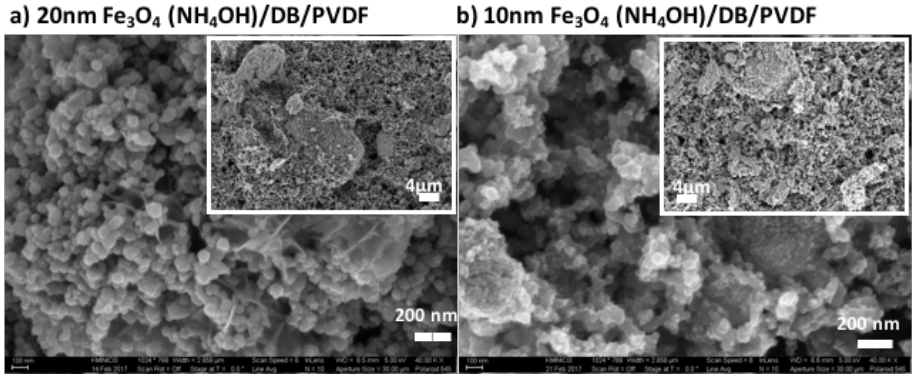

Figure 5-3: FE-SEM top view images of PVDF control electrodes.

5.2.2. Electrochemistry

From an electrochemical performance perspective, coin cells with a Li metal counter electrode were utilized and all the electrodes were prepared with Fe_3O_4 (or PEG-Fe_3O_4) active material, carbon additives, and polymeric binder in a 71.4:14.3:14.3 mass ratio. The mass ratio was chosen because in a previous study[1], the electrode exhibited its percolation threshold in electronic conductivity at this ratio. The electrolyte was 1 M $LiPF_6$ in ethylene carbonate (EC) and diethylene carbonate (DEC) (1:1 by weight).

Charging-discharging cycling (Figure 5-4) was conducted at a current density of 240 mA g^{-1} (~0.3 C) to determine capacity retention of the electrodes. The benefits of the PEG/PPBT

system are apparent for electrodes fabricated from either 10 nm or 20 nm Fe_3O_4 crystallites where the PEG-coating significantly enhanced cycling performance.

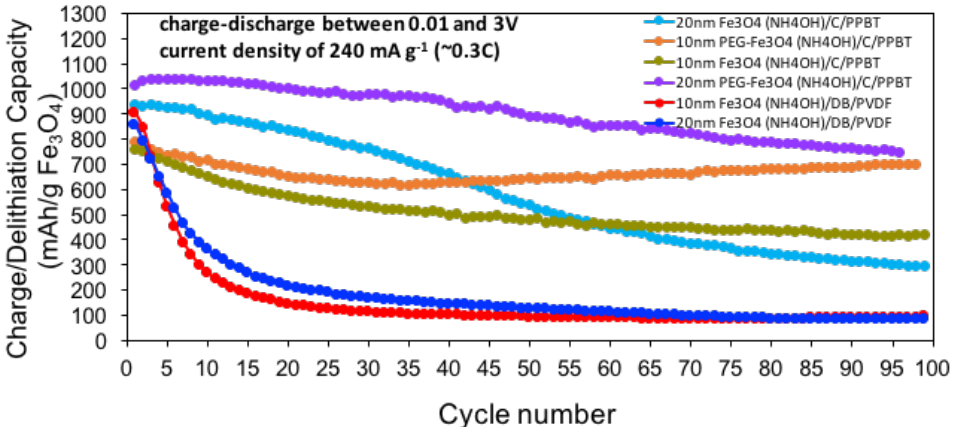

Figure 5-4: Cycling performance (capacity retention as a function of cycle number) collected for current density of 240 mA g^{-1} (~0.3C) between 0.01 and 3V

Exploring the impact of crystallite size, while the 20 nm PEG-Fe_3O_4 (NH_4OH)/PPBT electrode (purple line) initially had a higher capacity than the 10 nm PEG-Fe_3O_4 (NH_4OH)/PPBT alternative (orange line), it did not exhibit the same improved capacity retention over the course of 100 cycles. This initial capacity difference between 20 nm PEG-Fe_3O_4 (NH_4OH)/PPBT and 10 nm PEG-Fe_3O_4 (NH_4OH)/PPBT is ~200 mAh g^{-1} Fe_3O_4 (Table 5-1), which can be attributed to the differences in thickness and porosity of the electrodes. The results produced for electrochemical performance are not completely reproducible because of the inability to control thickness and porosity with the doctor blade during electrode fabrication.

Table 5-1: Initial discharge capacity values and capacity retention during cycling.

Electrode	Initial Charge/Delithiation Capacity (Figure 5-4)	Capacity Retention (%) After 100 Cycles (Figure 5-4)
10 nm Fe_3O_4 (NH_4OH)/PPBT	750 mAh/g Fe_3O_4	54 %
10 nm PEG-Fe_3O_4 (NH_4OH)/PPBT	790 mAh/g Fe_3O_4	89 %
20 nm Fe_3O_4 (NH_4OH)/PPBT	930 mAh/g Fe_3O_4	31 %
20 nm PEG-Fe_3O_4 (NH_4OH)/PPBT	1020 mAh/g Fe_3O_4	70 %
10 nm Fe_3O_4 (NH_4OH)/DB/PVDF	900 mAh/g Fe_3O_4	10 %
20 nm Fe_3O_4 (NH_4OH)/DB/PVDF	850 mAh/g Fe_3O_4	7.9 %

All PVDF electrodes had equally poor capacity retention over 100 cycles, which was expected. With regards to the effect of crystallite size, the 10 nm (ammonium hydroxide)/PVDF electrode (red line) had a slightly higher initial capacity as compared to the 20 nm (ammonium hydroxide)/PVDF electrode (blue line), which confirms the superior performance seen for the 10 nm crystallite size.

To further investigate battery performance, newly fabricated half cells were subjected to rate capability experiments (Figure 5-5), where cells were lithiated at a constant current density of 80 mA g^{-1} (~0.1C) and delithiated over a wide range of current densities (80 – 1600 mA g^{-1}) at a voltage range of 0.01 – 3 V. Overall, the PEG-Fe_3O_4/PPBT binder-based electrodes show much higher delithiated capacity than the PVDF control, which conveys its superior rate capability. Through rate capability testing, the 10 nm (ammonium hydroxide)/PPBT system (orange line) exhibited higher capacity and superior capacity retention compared to its 20 nm (ammonium hydroxide)/PPBT counterpart (purple line), which affirmed the cycling results (Figure 5-4).

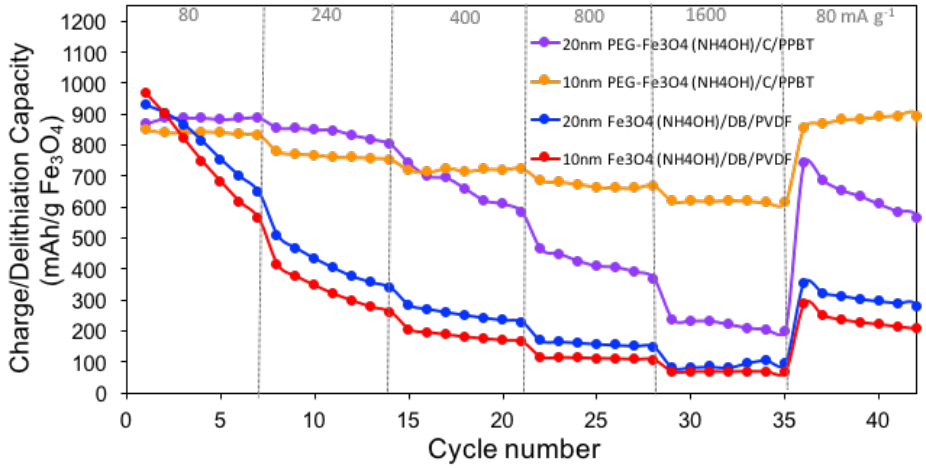

Figure 5-5: Delithiation rate capability, where cells were lithiated at a constant current density of 80 mA g^{-1} and delithiated at different current densities between 0.01 and 3V

EIS analysis presented in Figure 5-6 supports the cycling (Figure 5-4) and rate capability (Figure 5-5) data. The cells used in the EIS study correspond to those cycled between 0.01 and 3V as shown in Figure 5-4. Impedance testing was performed in the frequency range of 0.1 MHz to 0.1 Hz before cycling at 3V and after 100 cycles at their open-circuit voltage (OCV). Superior battery electrode performance can be attributed to decreased charge transfer resistance (R_{ct}), which is estimated from the diameter of the semicircle[78]. Initially, the charge transfer resistance was not effectively reduced in the PEG-PPBT vs. PVDF control system (Figure 5-6a). However, in their initial states, the 10 nm (ammonium hydroxide)/PPBT electrode (orange semicircle) exhibited lower charger transfer resistance than the 20 nm counterpart (purple semicircle), which support the expectation that smaller crystallites should afford superior performance.

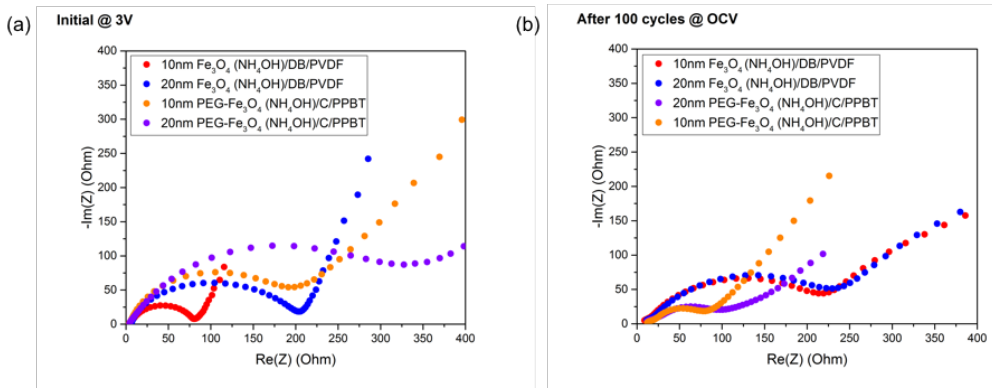

Figure 5-6: (a) Impedance spectra measured at 3V before cycling in the frequency range from 0.1 MHz to 0.1 Hz (b) Impedance spectra measured at open-circuit voltage (OCV) after 100 cycles in the frequency range from 0.1 MHz to 0.1 Hz

After 100 cycles (Figure 5-6b) the positive effects of introducing PEG/PPBT are clearly noticeable for the 'ammonium hydroxide' electrodes, where the charge transfer resistance decreased significantly, compared to the PVDF electrodes. EIS testing after 100 cycles further confirmed the performance advantages associated with the smaller, 10 nm crystallites, which supports the observations derived from cycling experiments (Figure 4-4). While it had been speculated that the charge transfer kinetics for composite electrodes fabricated from smaller crystallite sizes would be faster due to their greater surface area to volume ratio[59], the advantages of smaller crystallite size materials should be most apparent at higher current densities. This expectation was confirmed by the rate capability results presented in Figure 5-5.

5.2.3. Spectroscopic Characterization

Both electron and ion transport are known to be aided through molecular interactions between PPBT and Fe_3O_4 or PEG-Fe_3O_4.[2] Here, Fourier transform infrared (FT-IR) spectroscopy confirmed that PEG effectively interacts with and modifies the surface of Fe_3O_4 regardless of crystallite size (Figure 5-7).

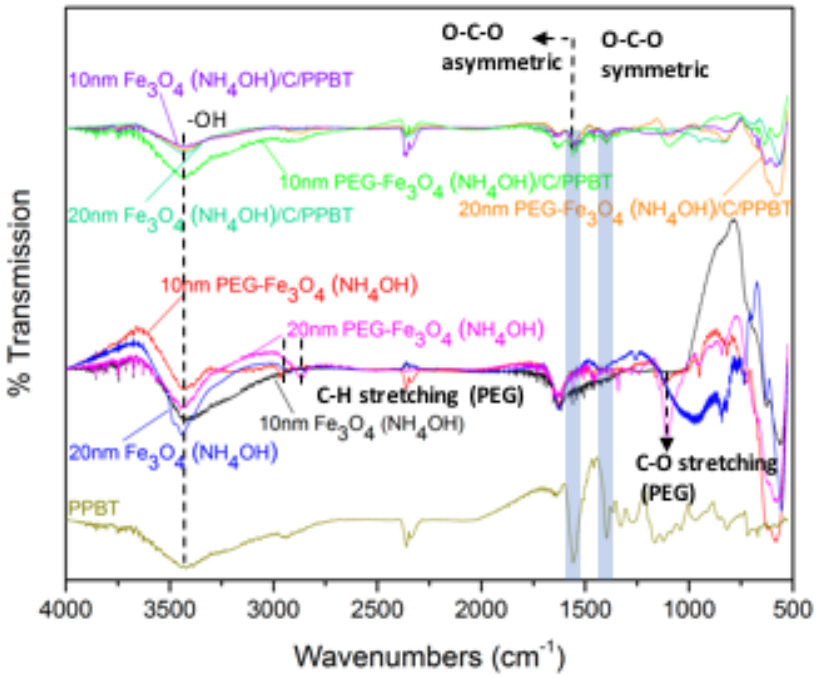

Figure 5-7: FT-IR spectra of materials (bottom lines: PPBT, Fe_3O_4, PEG-Fe_3O_4) and electrodes (upper lines: Fe_3O_4/C/PPBT, PEG-Fe_3O_4/C/PPBT).

Sharp C-H and C-O stretching bands at 2875 cm^{-1} and 1125 cm^{-1}, respectively, confirmed Fe_3O_4 surface modification with PEG[67]. FT-IR was further used to interrogate the chemical interactions within the composite electrodes. This was accomplished by first blending the requisite components, fabricating the electrodes and then scraping the resultant system to retrieve the powder material. All PPBT-based electrodes fabricated with all Fe_3O_4 and PEG-Fe_3O_4 samples, exhibited the stretching bands associated with the binder, PPBT; specifically, the carboxylate anion O-C-O asymmetric and symmetric stretching bands were observed at 1550 cm^{-1} and 1400 cm^{-1}, respectively[60,61,79,80] (Figure 5-7).

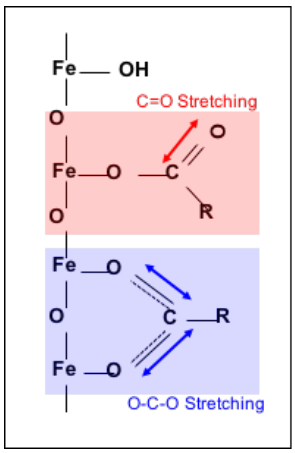

Figure 5-8: Proposed chemical structure of Fe_3O_4 in the electrode[2].

The 1760 cm^{-1} vibration previously described in Chapter 4 is not as clearly visible in the spectrum of electrode composites fabricated with the ammonium hydroxide derived magnetite. While the O-C-O asymmetric and stretching bands (Figure 5-7) are observed, the additional proposed Fe-carboxylate vibration is not present. Thus, the vibrational spectroscopy results suggest that the active material synthetic method is likely to impact the surface chemistry of the resultant materials and as a consequence bonding interactions between composite electrode components. These interactions may further play a significant role in determining electrode stability, a key factor that impacts battery performance. In the case of ammonium hydroxide, it is conceivable that the PPBT binder can interact with residual base residing on the surface of the nanoparticles, which might explain why the previously described Fe_3O_4-PPBT interactions (Figure 5-8) were not observed in the FTIR spectra of the ammonium hydroxide based electrodes (Figure 5-7).

XPS spectra of the C1s core level (Figure 5-9) further indicate the presence of chemical interactions. The bottom lines are spectra from the PEG-Fe_3O_4 powders of all samples, which exhibit a C-OH bond further confirming PEG surface modification to Fe_3O_4 particles[82]. The first

peak at ~285eV, exhibited in all PPBT-based electrodes, corresponds to the C-O bond[83]. The next peak at ~287eV is associated to the carboxylate (COO-) bond. The chemical shifts to a lower binding energy indicate an increase in interatomic distance, which could result from the additional bonding between PPBT and Fe_3O_4[84]. The remaining two peaks in the XPS spectra are associated to satellite peaks, which often result from extended delocalized electrons in a sample and provide evidence to π-π* interchain stacking along the PPBT backbone[85]. Such π-π* stacking may induce intermolecular charge transport, which leads to improved electrical properties of the PPBT binder system[2].

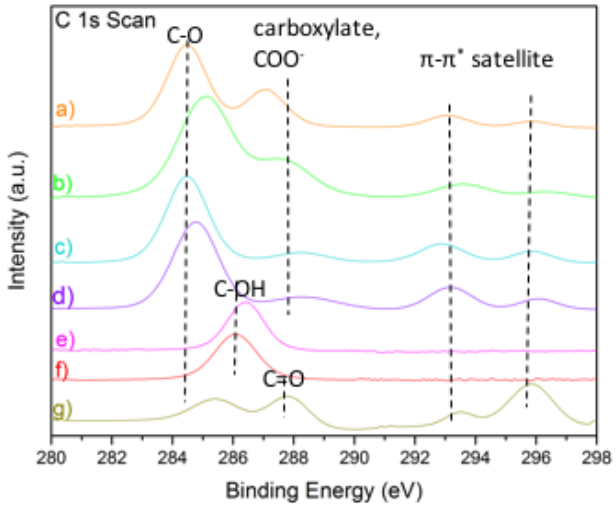

Figure 5-9: XPS spectra of C1s scan. (a) 20nm PEG-Fe_3O_4 (NH_4OH)/C/PPBT, (b) 10nm PEG-Fe_3O_4 (NH_4OH)/C/PPBT, (c) 20nm Fe_3O_4 (NH_4OH)/C/PPBT, (d) 10nm Fe_3O_4 (NH_4OH)/C/PPBT, (e) 20nm PEG-Fe_3O_4 (NH_4OH), (f) 10nm PEG-Fe_3O_4 (NH_4OH), (g) PPBT

XPS spectra of Fe 2p core level (Figure 5-10) provides additional information about the magnetite phase present in parent materials and electrodes. The first peak at ~712 eV corresponds to the Fe $2p_{3/2}$ core level electrons and the final peak at ~724 eV is associated with the Fe $2p_{1/2}$ core levels[86]. The remaining middle peak corresponds to Fe^{3+}, which when absent confirms a pure magnetite phase[82]. The presence of this peak would be further indication of

chemical interaction between PPBT carboxylic moieties and the Fe_3O_4 surface. The lack of this satellite peak further suggests the ammonium hydroxide derived electrodes do not exhibit chemical interactions indicative of electrode stability.

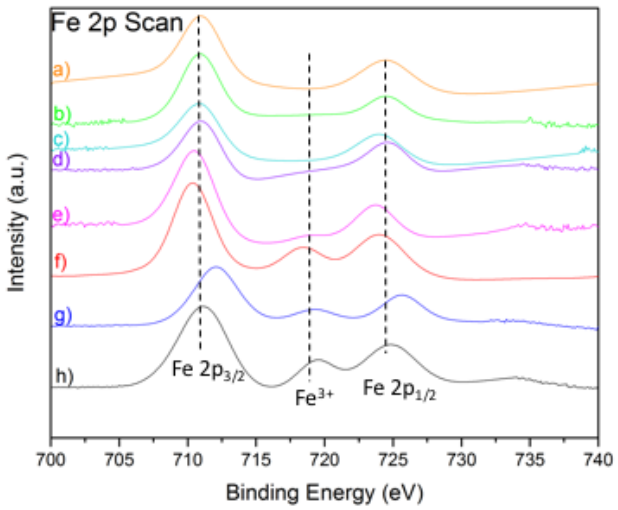

Figure 5-10: XPS spectra of Fe 2p scan of materials. (a) 20nm PEG-Fe_3O_4 (NH_4OH)/C/PPBT, (b) 10nm PEG-Fe_3O_4 (NH_4OH)/C/PPBT, (c) 20nm Fe_3O_4 (NH_4OH)/C/PPBT (d) 10nm Fe_3O_4 (NH_4OH)/C/PPBT, (e) 20nm PEG-Fe_3O_4 (NH_4OH), (f) 10nm PEG-Fe_3O_4 (NH_4OH), (g) 20nm Fe_3O_4 (NH_4OH), (h) 10nm Fe_3O_4 (NH_4OH)

5.3 Conclusion

The morphology was the same for all ammonium hydroxide derived electrodes, as indicated by SEM, which provided an analysis of crystallite size effects without additional factors. The ammonium hydroxide electrodes did not exhibit the previously described interactions between active material and polymeric binder, but crystallite size effects were analyzed from these systems. As previously reported[59,70], smaller crystallite size enhances electrochemical performance, as demonstrated by capacity retention, rate capability and decreased charge transfer resistance. From the first study of crystallite size effects in magnetite[90], nanocrystalline materials exhibited higher capacity, as a result of the smaller Li^+ diffusion path.

Furthermore, smaller crystallites exhibit faster charge transfer kinetics for composite electrodes[59], which supports their superior battery performance.

CHAPTER 6 : CONCLUSION AND FUTURE WORK

6.1 Conclusion

Materials dispersion is only one factor to consider when designing a composite electrode. As shown, the aggregate size is not indicative of battery performance. Electron and ion transport must also be considered, which is often dictated by surface chemistry and molecular interactions that allow for enhanced transport. The interactions between the binder and active material leads to electrode stability, which leads to improved capacity retention and decreased charge transfer resistance. A more dispersed morphology can lead to improvements in rate capability performance. Different surface chemistries, resulting from synthesis techniques utilizing different bases, lead to different morphologies and chemical interactions. Smaller crystallite size also aids in overall battery performance. It is crucial to consider how the active material synthesis can lead to enhanced battery performance during electrode fabrication. The results presented here show how the PEG/PPBT facile methodology for Fe_3O_4 anodes can further be improved by changes to the active material to produce high-capacity energy materials. The approaches described herein are expected to provide fundamental insights into the impact of active material synthesis on the design of battery electrodes, especially the crucial role of surface chemistry and its influence on interactions.

6.2 Future Directions

6.2.1 Extension of Crystallite Size and Surface Chemistry Study

Previously, collaborators at Stony Brook had the capabilities to make the 20 nm crystallite size using only the ammonium hydroxide base. Recently, their expertise allows them to synthesize 10 nm, 20 nm, and 30 nm crystallite sizes using the triethylamine base. An investigation into which of these crystallite sizes has enhanced cycling retention, rate capability

and reduced charge transfer resistance would provide a complete analysis into crystallite size effects on battery performance and confirm which size is best to use. Using the triethylamine base should ultimately show the smaller crystallite size has superior battery performance[59,70].

This work confirmed the importance of active material synthesis on the design of battery electrodes, particularly the crucial role of surface chemistry. Since surface chemistry is essential for enhancing interactions, it would be useful to investigate other synthesis methods and gain a wider repertoire. Collaborators at Stony Brook have indicated using other bases in their synthesis procedure, such as sulfides, which would provide useful information about potential interactions in the electrode system. A further understanding is still needed of why different bases produce distinct interactions and studying additional bases would provide a complete picture.

6.2.2 Further Investigations into PEG/PPBT System

The PEG/PPBT system has demonstrated improved capacity retention, rate capability and reduced charge transfer resistance after 100 cycles[2]. Part of the reason for this improved battery performance comes from the interactions between active material and polymeric binder that have been shown to improve electrode stability[60,61,92,93]. However, a fundamental understanding is needed to explain how the PEG/PPBT system works during cycling.

Recent advances using *in situ* TEM of electrochemistry allow insight into the inner-workings of a lithium ion battery during cycling[94]. *In situ* TEM would provide insight into whether the PEG/PPBT system is able to reduce the volume changes in the Fe_3O_4 anode. As previously discussed, a main limitation of magnetite as an active material stems from its poor cycling performance, due to the large volume changes that take place during repetitive charging-discharging[23]. This further analysis of the PEG/PPBT system would provide real time and atomic scale resolution during cycling to explain the mechanisms happening. *In situ* TEM is available at

Oakridge National Lab and Brookhaven National Lab, which would provide an accessible way to further investigate the PEG/PPBT system.

REFERENCES

(1) Kwon, Y. H.; Huie, M. M.; Choi, D.; Chang, M.; Marschilok, A. C.; Takeuchi, K. J.; Takeuchi, E. S.; Reichmanis, E. Toward Uniformly Dispersed Battery Electrode Composite Materials: Characteristics and Performance. *ACS Appl. Mater. Interfaces* **2016**, *8* (5), 3452–3463.

(2) Kwon, Y. H.; Minnici, K.; Huie, M. M.; Takeuchi, K. J.; Takeuchi, E. S.; Marschilok, A. C.; Reichmanis, E. Electron/Ion Transport Enhancer in High Capacity Li-Ion Battery Anodes. *Chem. Mater.* **2016**, *28* (18), 6689–6697.

(3) Goriparti, S.; Miele, E.; De Angelis, F.; Di Fabrizio, E.; Proietti Zaccaria, R.; Capiglia, C. Review on Recent Progress of Nanostructured Anode Materials for Li-Ion Batteries. *Journal of Power Sources*. July 2014, pp 421–443.

(4) Goodenough, J. B.; Park, K.-S. The Li-Ion Rechargeable Battery: A Perspective. *J. Am. Chem. Soc.* **2013**, *135* (4), 1167–1176.

(5) Tarascon, J.-M.; Armand, M. Issues and Challenges Facing Rechargeable Lithium Batteries. *Nature* **2001**, *414* (6861), 359–367.

(6) Armand, M.; Tarascon, J.-M. Building Better Batteries. *Nature* **2008**, *451* (7179), 652–657.

(7) Balogun, M. S.; Qiu, W.; Luo, Y.; Meng, H.; Mai, W.; Onasanya, A.; Olaniyi, T. K.; Tong, Y. A Review of the Development of Full Cell Lithium-Ion Batteries: The Impact of Nanostructured Anode Materials. *Nano Res.* **2016**, *9* (10), 2823–2851.

(8) Zhang, W.-M.; Wu, X.-L.; Hu, J.-S.; Guo, Y.-G.; Wan, L.-J. Carbon Coated Fe_3O_4 Nanospindles as a Superior Anode Material for Lithium-Ion Batteries. *Adv. Funct. Mater.* **2008**, *18* (24), 3941–3946.

(9) Lu, X.; Yu, M.; Wang, G.; Tong, Y.; Li, Y. Flexible Solid-State Supercapacitors: Design, Fabrication and Applications. *Energy Environ. Sci.* **2014**, *7* (7), 2160–2181.

(10) Qi Li, Caihong Xing, Zhaojie Wei, J. M. Enhanced Electrode Composition for Li Ion Battery. US 2011/0171371 A1, 2011.

(11) Balaya, P.; Li, H.; Kienle, L.; Maier, J. Fully Reversible Homogeneous and Heterogeneous Li Storage in RuO_2 with High Capacity. *Adv. Funct. Mater.* **2003**, *13* (8), 621–625.

(12) Tarascon, J.-M.; Armand, M. Issues and Challenges Facing Rechargeable Lithium Batteries. *Nature* **2001**, *414* (6861), 359–367.

(13) Yoon, T.; Kim, J.; Kim, J.; Lee, J. K. Electrostatic Self-Assembly of Fe_3O_4 Nanoparticles on Graphene Oxides for High Capacity Lithium-Ion Battery Anodes. *Energies* **2013**, *6* (9), 4830–4840.

(14) Chen, J.; Xu, L.; Li, W.; Gou, X. Alpha-Fe_2O_3 Nanotubes in Gas Sensor and Lithium-Ion Battery Applications. *Adv. Mater.* **2005**, *17* (5), 582–586.

(15) Poizot, P.; Laruelle, S.; Grugeon, S.; Dupont, L.; Tarascon, J.-M. Searching for New Anode Materials for the Li-Ion Technology: Time to Deviate from the Usual Path. *J. Power Sources* **2001**, *97–98*, 235–239.

(16) Tarascon, J.-M.; Poizot, P.; Laruelle, S.; Grugeon, S.; Dupont, L. Nano-Sized Transition-Metal Oxides as Negative-Electrode Materials forLithium-Ion Batteries. *Nature* **2000**, *407* (6803), 496–499.

(17) Zhang, W.-M.; Wu, X.-L.; Hu, J.-S.; Guo, Y.-G.; Wan, L.-J. Carbon Coated Fe_3O_4 Nanospindles as a Superior Anode Material for Lithium-Ion Batteries. *Adv. Funct. Mater.* **2008**, *18* (24), 3941–3946.

(18) Ito, S.; Nakaoka, K.; Kawamura, M.; Ui, K.; Fujimoto, K.; Koura, N. Lithium Battery Having a Large Capacity Using Fe_3O_4 as a Cathode Material. *J. Power Sources* **2005**, *146* (1–2), 319–322.

(19) Taberna, P. L.; Mitra, S.; Poizot, P.; Simon, P.; Tarascon, J.-M. High Rate Capabilities Fe_3O_4-Based Cu Nano-Architectured Electrodes for Lithium-Ion Battery Applications. *Nat. Mater.* **2006**, *5* (7), 567–573.

(20) Mitra, S.; Poizot, P.; Finke, A.; Tarascon, J.-M. Growth and Electrochemical Characterization versus Lithium of Fe_3O_4 Electrodes Made by Electrodeposition. *Adv. Funct. Mater.* **2006**, *16* (17), 2281–2287.

(21) Wu, Y.; Zhan, L.; Huang, K.; Wang, H.; Yu, H.; Wang, S.; Peng, F.; Lai, C. Iron Based Dual-Metal Oxides on Graphene for Lithium-Ion Batteries Anode: Effects of Composition and Morphology. *J. Alloys Compd.* **2016**, *684*, 47-54.

(22) Lian, P.; Zhu, X.; Xiang, H.; Li, Z.; Yang, W.; Wang, H. Enhanced Cycling Performance of Fe_3O_4–graphene Nanocomposite as an Anode Material for Lithium-Ion Batteries. *Electrochim. Acta* **2010**, *56* (2), 834–840.

(23) Yu, Y.; Chen, C.-H.; Shi, Y. A Tin-Based Amorphous Oxide Composite with a Porous, Spherical, Multideck-Cage Morphology as a Highly Reversible Anode Material for Lithium-Ion Batteries. *Adv. Mater.* **2007**, *19* (7), 993–997.

(24) Huang, X.; Zhou, X.; Qian, K.; Zhao, D.; Liu, Z.; Yu, C. A Magnetite Nanocrystal/graphene Composite as High Performance Anode for Lithium-Ion Batteries. *J. Alloys Compd.* **2011**, *514*, 76–80.

(25) Zhang, Y.; Li, Y.; Li, H.; Zhao, Y.; Yin, F.; Bakenov, Z. Electrochemical Performance of Carbon-Encapsulated Fe_3O_4 Nanoparticles in Lithium-Ion Batteries: Morphology and Particle Size Effects. *Electrochim. Acta* **2016**, *216*, 475–483.

(26) Zhang, W.-M.; Wu, X.-L.; Hu, J.-S.; Guo, Y.-G.; Wan, L.-J. Carbon Coated Fe_3O_4 Nanospindles as a Superior Anode Material for Lithium-Ion Batteries. *Adv. Funct. Mater.* **2008**, *18* (24), 3941–3946.

(27) Ban, C.; Wu, Z.; Gillaspie, D. T.; Chen, L.; Yan, Y.; Blackburn, J. L.; Dillon, A. C. Nanostructured Fe_3O_4/SWNT Electrode: Binder-Free and High-Rate Li-Ion Anode. *Adv. Mater.* **2010**, *22* (20), E145–E149.

(28) He, Y.; Huang, L.; Cai, J.-S.; Zheng, X.-M.; Sun, S.-G. Structure and Electrochemical Performance of Nanostructured Fe_3O_4/carbon Nanotube Composites as Anodes for Lithium Ion Batteries. *Electrochim. Acta* **2010**, *55* (3), 1140–1144.

(29) Bruck, A. M.; Cama, C. A.; Gannett, C. N.; Marschilok, A. C.; Takeuchi, E. S.; Takeuchi, K. J. Nanocrystalline Iron Oxide Based Electroactive Materials in Lithium Ion Batteries: The Critical Role of Crystallite Size, Morphology, and Electrode Heterostructure on Battery Relevant Electrochemistry. *Inorg. Chem. Front.* **2016**, *3* (1), 26–40.

(30) Aurbach, D.; Levi, M. D.; Levi, E.; Schechter, A. Failure and Stabilization Mechanisms of Graphite Electrodes. *J. Phys. Chem. B* **1997**, *101* (12), 2195–2206.

(31) Needham, S. a.; Wang, G. X.; Konstantinov, K.; Tournayre, Y.; Lao, Z.; Liu, H. K. Electrochemical Performance of Co_3O_4–C Composite Anode Materials. *Electrochem. Solid-State Lett.* **2006**, *9* (7), A315.

(32) Hu, J.; Li, H.; Huang, X.; Chen, L. Improve the Electrochemical Performances of Cr_2O_3 Anode for Lithium Ion Batteries. *Solid State Ionics* **2006**, *177* (26–32 SPEC. ISS.), 2791–2799.

(33) Xu, J.; Yang, H.; Fu, W.; Du, K.; Sui, Y.; Chen, J.; Zeng, Y.; Li, M.; Zou, G. Preparation and Magnetic Properties of Magnetite Nanoparticles by Sol–gel Method. *J. Magn. Magn. Mater.* **2007**, *309* (2), 307–311.

(34) Teo, B. M.; Chen, F.; Hatton, T. A.; Grieser, F.; Ashokkumar, M. Novel One-Pot Synthesis of Magnetite Latex Nanoparticles by Ultrasound Irradiation. *Langmuir* **2009**, *25* (5), 2593–2595.

(35) Lee, Y.; Lee, J.; Bae, C. J.; Park, J.-G.; Noh, H.-J.; Park, J.-H.; Hyeon, T. Large-Scale Synthesis of Uniform and Crystalline Magnetite Nanoparticles Using Reverse Micelles as Nanoreactors under Reflux Conditions. *Adv. Funct. Mater.* **2005**, *15* (3), 503–509.

(36) Mizutani, N.; Iwasaki, T.; Watano, S.; Yanagida, T.; Kawai, T. Size Control of Magnetite Nanoparticles in Hydrothermal Synthesis by Coexistence of Lactate and Sulfate Ions.

Curr. Appl. Phys. **2010**, *10* (3), 801–806.

(37) Su, M.; He, C.; Shih, K. Facile Synthesis of Morphology and Size-Controlled α-Fe_2O_3 and Fe_3O_4 Nano-and Microstructures by Hydrothermal/solvothermal Process: The Roles of Reaction Medium and Urea Dose. *Ceram. Int.* **2016**, *42* (13), 14793–14804.

(38) Sun, X.; Zheng, C.; Zhang, F.; Yang, Y.; Wu, G.; Yu, A.; Guan, N. Size-Controlled Synthesis of Magnetite (Fe_3O_4) Nanoparticles Coated with Glucose and Gluconic Acid from a Single Fe(III) Precursor by a Sucrose Bifunctional Hydrothermal Method. *J. Phys. Chem. C* **2009**, *113* (36), 16002–16008.

(39) Li, D.; Jiang, D.; Chen, M.; Xie, J.; Wu, Y.; Dang, S.; Zhang, J. An Easy Fabrication of Monodisperse Oleic Acid-Coated Fe_3O_4 Nanoparticles. *Mater. Lett.* **2010**, *64* (22).

(40) Guardia, P.; Batlle-Brugal, B.; Roca, A. G.; Iglesias, O.; Morales, M. P.; Serna, C. J.; Labarta, A.; Batlle, X. Surfactant Effects in Magnetite Nanoparticles of Controlled Size. *J. Magn. Magn. Mater.* **2007**, *316*, 756–759.

(41) Zhang, L.; He, R.; Gu, H.-C. Oleic Acid Coating on the Monodisperse Magnetite Nanoparticles. *Appl. Surf. Sci.* **2006**, *253* (5), 2611–2617.

(42) Sun, S.; Murray, C. B.; Weller, D.; Folks, L.; Moser, A. Monodisperse FePt Nanoparticles and Ferromagnetic FePt Nanocrystal Superlattices. *Science*. **2000**, *287* (5460), 1989-92.

(43) Xiong, Q. Q.; Tu, J. P.; Lu, Y.; Chen, J.; Yu, Y. X.; Qiao, Y. Q.; Wang, X. L.; Gu, C. D. Synthesis of Hierarchical Hollow-Structured Single-Crystalline Magnetite (Fe_3O_4) Microspheres: The Highly Powerful Storage versus Lithium as an Anode for Lithium Ion Batteries. *J. Phys. Chem. C.* **2012**, *116* (10).

(44) Baaziz, W.; Pichon, B. P.; Fleutot, S.; Liu, Y.; Lefevre, C.; Greneche, J. M.; Toumi, M.; Mhiri, T.; Begin-Colin, S. Magnetic Iron Oxide Nanoparticles: Reproducible Tuning of the Size and Nanosized-Dependent Composition, Defects, and Spin Canting. *J. Phys. Chem. C* **2014**, *118* (7).

(45) Sun, S.; Zeng, H. Size-Controlled Synthesis of Magnetite Nanoparticles. *J. Am. Chem. Soc.* **2002**, *124*, 8204–8205.

(46) Li, Z.; Chen, H.; Bao, H.; Gao, M. One-Pot Reaction to Synthesize Water-Soluble Magnetite Nanocrystals. *Chem. Soc. J. Colloid Interface Sci Int. J. Pharm. J. Magn. Magn. Mater. Sci. Angew. Chem., Int. Ed. J. W. M.; Brooks, R. A. Sci. Clin. Appl. Magn. Carriers Chem. Mater* **2002**, *31* (15), 118–215.

(47) Peng, S.; Wang, C.; Xie, J.; Sun, S. Synthesis and Stabilization of Monodisperse Fe Nanoparticles. *J. Am. Chem. Soc.* **2006**, *128* (33), 10676-10677.

(48) Liu, J.; Wu, Z.; Tian, Q.; Wu, W.; Xiao, X. Shape-Controlled Iron Oxide Nanocrystals:

Synthesis, Magnetic Properties and Energy Conversion Applications. *CrystEngComm*. **2014**, *18*, 6303.

(49) Petcharoen, K.; Sirivat, A. Synthesis and Characterization of Magnetite Nanoparticles via the Chemical Co-Precipitation Method. *Mater. Sci. Eng. B* **2012**, *177* (5), 421–427.

(50) Hu, D.; Wang, Y.; Song, Q. Weakly Magnetic Field-Assisted Synthesis of Magnetite Nano-Particles in Oxidative Co-Precipitation. *Particuology* **2009**, *7* (5), 363–367.

(51) Anbarasu, M.; Anandan, M.; Chinnasamy, E.; Gopinath, V.; Balamurugan, K. Synthesis and Characterization of Polyethylene Glycol (PEG) Coated Fe_3O_4 Nanoparticles by Chemical Co-Precipitation Method for Biomedical Applications. *Spectrochim. Acta. A. Mol. Biomol. Spectrosc.* **2015**, *135*, 536–539.

(52) Valenzuela, R.; Fuentes, M. C.; Parra, C.; Baeza, J.; Duran, N.; Sharma, S. K.; Knobel, M.; Freer, J. Influence of Stirring Velocity on the Synthesis of Magnetite Nanoparticles (Fe_3O_4) by the Co-Precipitation Method. *J. Alloys Compd.* **2009**, *488* (1), 227–231.

(53) Mascolo, M.; Pei, Y.; Ring, T. Room Temperature Co-Precipitation Synthesis of Magnetite Nanoparticles in a Large pH Window with Different Bases. *Materials (Basel)*. **2013**, *6* (12), 5549–5567.

(54) Shen, L.; Qiao, Y.; Guo, Y.; Meng, S.; Yang, G.; Wu, M.; Zhao, J. Facile Co-Precipitation Synthesis of Shape-Controlled Magnetite Nanoparticles. *Ceram. Int.* **2014**, *40* (1), 1519–1524.

(55) Colloids; Surfaces, A.; Physicochem; Eng. Simple and Novel Strategies to Achieve Shape and Size Control of Magnetite Nanoparticles Intended for Biomedical Applications. *Aspects* **2016**, *504*, 320–330.

(56) Peternele, W. S.; Monge Fuentes, V.; Fascineli, M. L.; Rodrigues da Silva, J.; Silva, R. C.; Lucci, C. M.; Bentes de Azevedo, R. Experimental Investigation of the Coprecipitation Method: An Approach to Obtain Magnetite and Maghemite Nanoparticles with Improved Properties. *J. Nanomater.* **2014**, 1–10.

(57) Posada, J. O. G.; Rennie, A. J. R.; Villar, S. P.; Martins, V. L.; Marinaccio, J.; Barnes, A.; Glover, C. F.; Worsley, D. A.; Hall, P. J. Aqueous Batteries as Grid Scale Energy Storage Solutions. *Renew. Sustain. Energy Rev.* **2017**, *68*, 1174–1182.

(58) Gnanaprakash, G.; Mahadevan, S.; Jayakumar, T.; Kalyanasundaram, P.; Philip, J.; Raj, B. Effect of Initial pH and Temperature of Iron Salt Solutions on Formation of Magnetite Nanoparticles. *Mater. Chem. Phys.* **2007**, *103* (1), 168–175.

(59) Zhu, S.; Marschilok, A. C.; Takeuchi, E. S.; Yee, G. T.; Wang, G.; Takeuchi, K. J. Nanocrystalline Magnetite: Synthetic Crystallite Size Control and Resulting Magnetic and Electrochemical Properties. *J. Electrochem. Soc.* **2010**, *157* (11), A1158.

(60) Kovalenko, I.; Zdyrko, B.; Magasinski, a.; Hertzberg, B.; Milicev, Z.; Burtovyy, R.; Luzinov, I.; Yushin, G. A Major Constituent of Brown Algae for Use in High-Capacity Li-Ion Batteries. *Science.* **2011**, *334* (6052), 75–79.

(61) Mazouzi, D.; Lestriez, B.; Roué, L.; Guyomard, D. Silicon Composite Electrode with High Capacity and Long Cycle Life. *Electrochem. Solid-State Lett.* **2009**, *12* (11), A215.

(62) Magasinski, A.; Zdyrko, B.; Kovalenko, I.; Hertzberg, B.; Burtovyy, R.; Huebner, C. F.; Fuller, T. F.; Luzinov, I.; Yushin, G. Toward Efficient Binders for Li-Ion Battery Si-Based Anodes: Polyacrylic Acid. *ACS Appl. Mater. Interfaces* **2010**, *2* (11), 3004–3010.

(63) Bridel, J.-S.; Azaïs, T.; Morcrette, M.; Tarascon, J.-M.; Larcher, D. Key Parameters Governing the Reversibility of Si/Carbon/CMC Electrodes for Li-Ion Batteries. *Chem. Mater.* **2010**, *22* (3), 1229–1241.

(64) Mukhopadhyay, A.; Joshi, N.; Chattopadhyay, K.; De, G. A Facile Synthesis of PEG-Coated Magnetite (Fe_3O_4) Nanoparticles and Their Prevention of the Reduction of Cytochrome C. *ACS Appl. Mater. Interfaces* **2012**, *4* (1), 142–149.

(65) Tai, M. F.; Lai, C. W.; Hamid, S. B. A. Facile Synthesis Polyethylene Glycol Coated Magnetite Nanoparticles for High Colloidal Stability. *J. Nanomater.* **2016**, 1–7.

(66) Chou, S.-L.; Pan, Y.; Wang, J.-Z.; Liu, H.-K.; Dou, S.-X. Small Things Make a Big Difference: Binder Effects on the Performance of Li and Na Batteries. *Phys. Chem. Chem. Phys. Phys. Chem. Chem. Phys* **2014**, *16* (16), 20347–20359.

(67) Mukhopadhyay, A.; Joshi, N.; Chattopadhyay, K.; De, G. A Facile Synthesis of PEG-Coated Magnetite (Fe_3O_4) Nanoparticles and Their Prevention of the Reduction of Cytochrome C. *ACS Appl. Mater. Interfaces* **2012**, *4* (1), 142–149.

(68) Itoh, H.; Sugimoto, T. Systematic Control of Size, Shape, Structure, and Magnetic Properties of Uniform Magnetite and Maghemite Particles. *J. Colloid Interface Sci.* **2003**, *265* (2), 283–295.

(69) Si, S.; Kotal, A.; Mandal, T. K.; Giri, S.; Nakamura, H.; Kohara, T. Size-Controlled Synthesis of Magnetite Nanoparticles in the Presence of Polyelectrolytes. *Chem. Mater.* **2004**, *16* (18), 3489–3496.

(70) Zhu, S.; Marschilok, A. C.; Takeuchi, E. S.; Takeuchi, K. J. Crystallite Size Control and Resulting Electrochemistry of Magnetite, Fe_3O_4. *Electrochem. Solid-State Lett.* **2009**, *12* (4), A91–A94.

(71) Hajdú, A.; Illés, E.; Tombácz, E.; Borbáth, I. Surface Charging, Polyanionic Coating and Colloid Stability of Magnetite Nanoparticles. *Colloids Surfaces A Physicochem. Eng. Asp.* **2009**, *347* (1–3), 104–108.

(72) Liu, J.; Zhao, Z.; Jiang, G. Coating Fe_3O_4 Magnetic Nanoparticles with Humic Acid for High Efficient Removal of Heavy Metals in Water. *Environ. Sci. Technol.* **2008**, *42* (18), 6949–6954.

(73) Tantra, R.; Schulze, P.; Quincey, P. Effect of Nanoparticle Concentration on Zeta-Potential Measurement Results and Reproducibility. *Particuology* **2010**, *8* (3), 279–285.

(74) Márquez, F.; Campo, T.; Cotto, M.; Polanco, R.; Roque, R.; Fierro, P.; Sanz, J. M.; Elizalde, E.; Morant, C. Synthesis and Characterization of Monodisperse Magnetite Hollow Microspheres. *Soft Nanosci. Lett.* **2011**, *1*, 25–32

.

(75) Ma, F.-X.; Hu, H.; Wu, H. Bin; Xu, C.-Y.; Xu, Z.; Zhen, L.; David Lou, X. W. Formation of Uniform Fe_3O_4 Hollow Spheres Organized by Ultrathin Nanosheets and Their Excellent Lithium Storage Properties. *Adv. Mater.* **2015**, *27* (27), 4097–4101.

(76) Su, D.; Horvat, J.; Munroe, P.; Ahn, H.; Ranjbartoreh, A. R.; Wang, G. Polyhedral Magnetite Nanocrystals with Multiple Facets: Facile Synthesis, Structural Modelling, Magnetic Properties and Application for High Capacity Lithium Storage. *Chem. - A Eur. J.* **2012**, *18* (2), 488–497.

(77) Wang, Q.; Chen, D.; Chen, J.; Lai, C.; Li, L.; Wang, C. Facile Synthesis and Electrochemical Properties of Fe_3O_4 Hexahedra for Li-Ion Battery Anode. *Mater. Lett.* **2015**, *141*, 319–322.

(78) Jow, T. R.; Shacklette, L. W. Electrochemical Characteristics of Alkali-Metal Doped Polyacetylene Electrodes. *J. Electrochem. Soc.* **1988**, *135* (3), 541.

(79) Nappini, S.; Magnano, E.; Bondino, F.; Píš, I.; Barla, A.; Fantechi, E.; Pineider, F.; Sangregorio, C.; Vaccari, L.; Venturelli, L.; Baglioni, P. Surface Charge and Coating of $CoFe_2O_4$ Nanoparticles: Evidence of Preserved Magnetic and Electronic Properties. *J. Phys. Chem. C* **2015**, *119* (45), 25529–25541.

(80) Nappini, S.; Bonini, M.; Bombelli, F. B.; Pineider, F.; Sangregorio, C.; Baglioni, P.; Nordèn, B. Controlled Drug Release under a Low Frequency Magnetic Field: Effect of the Citrate Coating on Magnetoliposomes Stability. *Soft Matter* **2011**, *7* (3), 1025–1037.

(81) Zhang, G.; Kim, G.; Choi, W. Visible Light Driven Photocatalysis Mediated via Ligand-to-Metal Charge Transfer (LMCT): An Alternative Approach to Solar Activation of Titania. *Energy Environ. Sci.* **2014**, *7* (3), 954.

(82) Yang, J.; Zou, P.; Yang, L.; Cao, J.; Sun, Y.; Han, D.; Yang, S.; Wang, Z.; Chen, G.; Wang, B.; Kong, X. A Comprehensive Study on the Synthesis and Paramagnetic Properties of PEG-Coated Fe_3O_4 Nanoparticles. *Appl. Surf. Sci.* **2014**, *303*, 425–432.

(83) Moreno-Castilla, C.; López-Ramón, M. .; Carrasco-Marín, F. Changes in Surface Chemistry of Activated Carbons by Wet Oxidation. *Carbon N. Y.* **2000**, *38* (14), 1995–

2001.

(84) Fujii, T.; De Groot, F. M. F.; Sawatzky, G. A.; Voogt, F. C.; Hibma, T.; Okada, K. In Situ XPS Analysis of Various Iron Oxide Films Grown by NO_2-Assisted Molecular-Beam Epitaxy. *Phys. Rev. B* **1998**, *59*, 3195–3202.

(85) XPS Interpretation of Carbon http://xpssimplified.com/elements/carbon.php (accessed Mar 5, 2017).

(86) Bhargava, G.; Gouzman, I.; Chun, C. M.; Ramanarayanan, T. A.; Bernasek, S. L. Characterization of the "native" Surface Thin Film on Pure Polycrystalline Iron: A High Resolution XPS and TEM Study. *Appl. Surf. Sci.* **2007**, *253* (9), 4322–4329.

(87) Vayssières, L.; Chanéac, C.; Tronc, E.; Jolivet, J. P. Size Tailoring of Magnetite Particles Formed by Aqueous Precipitation: An Example of Thermodynamic Stability of Nanometric Oxide Particles. *J. Colloid Interface Sci.* **1998**, *205* (2), 205–212.

(88) Gnanaprakash, G.; Mahadevan, S.; Jayakumar, T.; Kalyanasundaram, P.; Philip, J.; Raj, B. Effect of Initial pH and Temperature of Iron Salt Solutions on Formation of Magnetite Nanoparticles. *Mater. Chem. Phys.* **2007**, *103* (1), 168–175.

(89) Yu, W.-G.; Zhang, T.-L.; Qiao, X.-J.; Zhang, J.-G.; Yang, L. Effects of Synthetical Conditions on Octahedral Magnetite Nanoparticles. *Mater. Sci. Eng. B* **2007**, *136* (2–3), 101–105.

(90) Komaba, S.; Mikumo, T.; Ogata, A. Electrochemical Activity of Nanocrystalline Fe_3O_4 in Aprotic Li and Na Salt Electrolytes. *Electrochem. Commun.* **2008**, *10*, 1276–1279.

(91) Tarascon, J.-M.; Poizot, P.; Laruelle, S.; Grugeon, S.; Dupont, L. Nano-Sized Transition-Metal Oxides as Negative-Electrode Materials for Lithium-Ion Batteries. *Nature* **2000**, *407* (6803), 496–499.

(92) Magasinski, A.; Zdyrko, B.; Kovalenko, I.; Hertzberg, B.; Burtovyy, R.; Huebner, C. F.; Fuller, T. F.; Luzinov, I.; Yushin, G. Toward Efficient Binders for Li-Ion Battery Si-Based Anodes: Polyacrylic Acid. *ACS Appl. Mater. Interfaces* **2010**, *2* (11), 3004–3010.

(93) Bridel, J. S.; Azaïs, T.; Morcrette, M.; Tarascon, J. M.; Larcher, D. Key Parameters Governing the Reversibility of Si/carbon/CMC Electrodes for Li-Ion Batteries. *Chem. Mater.* **2010**, *22* (3), 1229–1241.

(94) Hua Liu, X.; Yu Huang, J. In Situ TEM Electrochemistry of Anode Materials in Lithium Ion Batteries. *Energy Environ. Sci. Energy Environ. Sci* **2011**, *3844* (4), 3844–3860.